

## Appendix E

### Wild Rose Petrophysics

#### Table of Contents

Objectives .....	2
Stratigraphy.....	3
Petrophysics.....	4
Net Mean Stress.....	4
Core Data .....	5
Temperature Curve .....	7
Pressure Curve .....	7
Curve Normalization.....	7
Vshale – Vclay.....	7
Porosity .....	9
Vshale-Porosity Transform .....	13
Cased Hole Pulsed Neutron Logs .....	23
Coal Flag.....	27
Permeability .....	28
Water Resistivity .....	30
Water Saturation .....	44
TDT Resistivity .....	51
Cutoffs.....	52
Flow Units .....	52
Conclusions.....	54

## Objectives

Petro Data Integration, LLC, was contracted by Advanced Resources International (ARI), Denver office, to supply petrophysical and geoscience consulting in support of the water remediation and enhanced gas recovery project in the Greater Green River and Wind River Basins.

The United States Department of Energy (DE-FC-02NT41437) funded this project. British Petroleum provided data, and Schlumberger Oilfield Services gave technical support.

The overall goal of the project was to process petrophysics for wells in the 18N, 94W township of the Wild Rose Field, and look for methods to distinguish water from gas. Work commenced on August 11, 2004, and was completed by October 1, 2004.

Petro Data Integration worked closely with personnel from Advanced Resources International on all aspects of the project. The objectives of the study were as follows.

- Build a petrophysical model for clay volume, porosity, permeability, and water saturation based on openhole log suites and core data.
  - Review prior petrophysics and revise/incorporate where appropriate.
- Calibrate cased hole pulsed neutron log response (TDT) to the petrophysical models developed for the openhole logs.
- Correct core data to in situ reservoir pressure conditions, and shift relative to logs.
- Utilize log suites to distinguish between gas and low salinity formation water.
- Define and distribute flow units based on stratigraphy, facies and petrophysical characteristics.
- Export summations for incorporation into a reservoir simulation model.

## Stratigraphy

The target of this study is the Almond formation of the Mesaverde group (fig. E-1). It is composed of stacked, laterally discontinuous estuarine sands interbedded with coal, siltstone and shale. In general, individual sands are thin (1-20 feet), coarsening upward sequences. Local channels do occur and are cleaner, higher quality reservoir.

*Within* the Almond formation is a prominent flooding surface (ALMD\_SH2), which can be correlated across the study area.

*Above* the Almond is the Lewis formation, which is a marine shale/siltstone sequence that forms the upper seal of the gas sands. A characteristic high gamma ray “hot” bentonite shale is in the upper part of the sequence (L-Marker), and is a prominent stratigraphic marker and seismic horizon.

*Below* the Almond formation is the Ericson formation. It is characterized by cleaner, more porous fluvial channel sands, but tests wet in the Wild Rose Field study area.

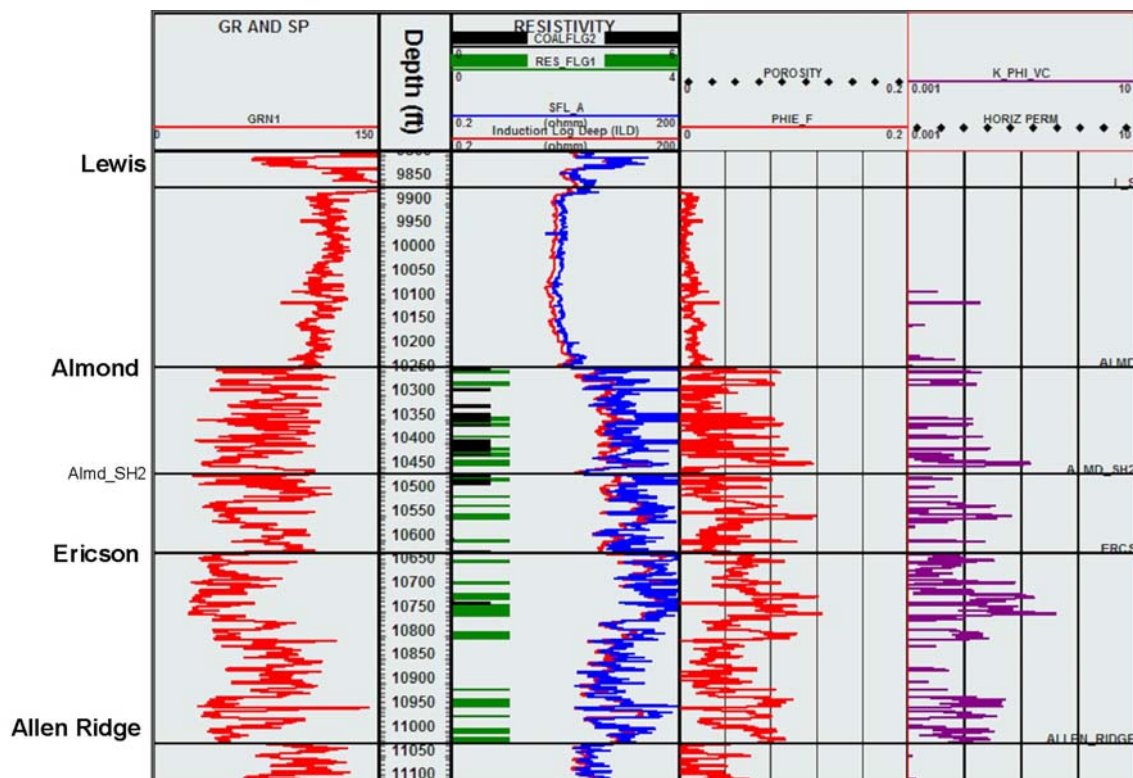


**Fig. E-1. Major stratigraphy**

## Petrophysics

Petro Data Integration conducted log analyses and petrophysical modeling using the Terrasciences software suite. Schlumberger Oilfield Services provided petrophysical consulting.

A total of 104 wells were loaded and screened for petrophysics. Seventy-one had openhole logs and thirty-seven had cased hole logs. Of these, five had both cased and openhole logs and eleven wells were cored. Eighty-five wells were fully processed for petrophysics. Fifteen of the eighteen wells that were not processed were cased hole logs with limited or poor data sets.

### Net Mean Stress

At depth, the core is under a significant confining pressure. The core expands and cracks develop as it is brought to the surface. As a result, core data taken under stress that is significantly less than subsurface conditions may record optimistically high permeability due to crack expansion. Porosity is less affected. The present net mean stress of the reservoir is calculated using the equations in Table E-1.

**Table E-1. Equation: calculation of present net mean stress of the reservoir**

$\text{Overburden (psi)} = \text{depth (ft)} * 1 \text{ psi/ft}$ $\text{Effective Vertical Stress (EVS)} = \text{Overburden (psi)} - \text{Reservoir Pressure (psi)}$ $\text{Effective Horizontal Stress (EHS)} = \text{EVS} * (\nu / (1 - \nu)); \nu = \text{Poisson's Ratio}$ $\text{Net Mean Stress (nms)} = (\text{EVS} + (2 * \text{EHS})) / 3$
--

This method is an approximation of in situ reservoir stress and assumes that horizontal stress is equal in the two principal component directions. It then averages the three main calculated principle stress components to obtain an estimation of the confining pressure needed for core measurements. Poisson's ratio is estimated to be 0.21, true vertical depth ranges 9,300-10,400 feet, and reservoir pressure is approximately 5,300 psi.

As a result, the net mean stress for these rocks is approximately 2,000-2,600 psi depending on the depth of the reservoir.

## Core Data

Most core data provided was taken at 800 psi. Core data under 2,000 to 2,600 psi confining pressure was obtained in Champlin 276, Standard Draw 3-16, Overland 43-6, Siberia Ridge 1, Siberia Ridge 5, and Siberia Ridge 5-2.

Based on these data, the porosity correction to core at net mean stress of 2,000-2,600 psi is shown in fig. E-2.

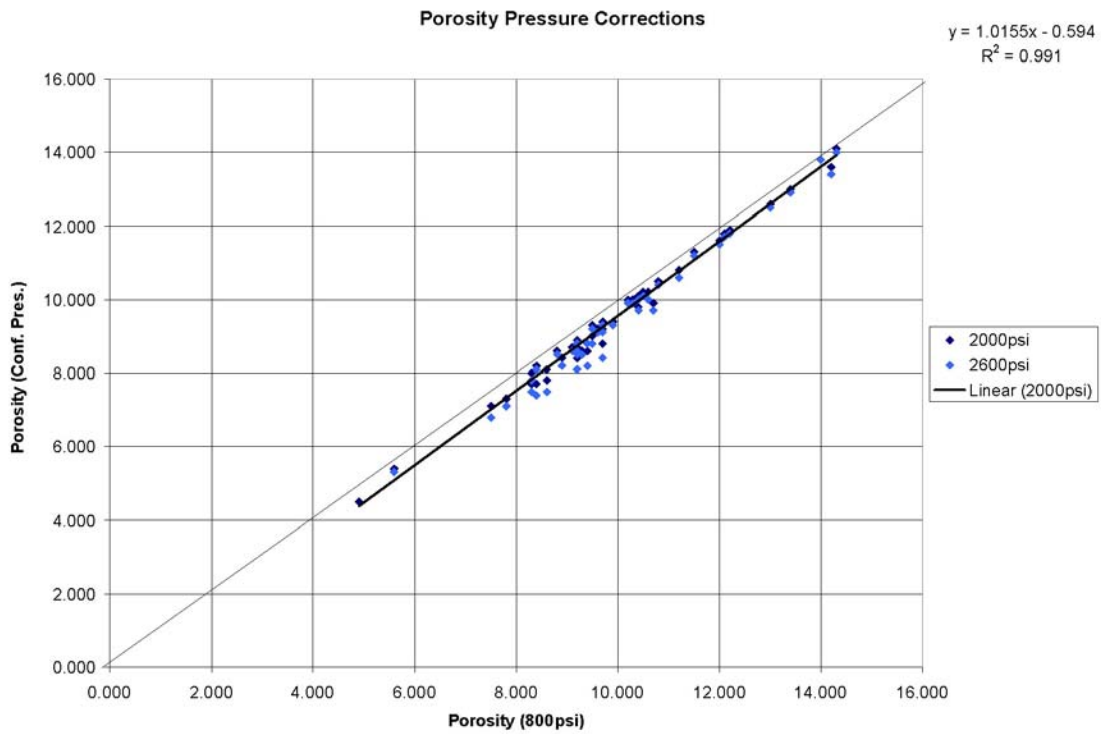
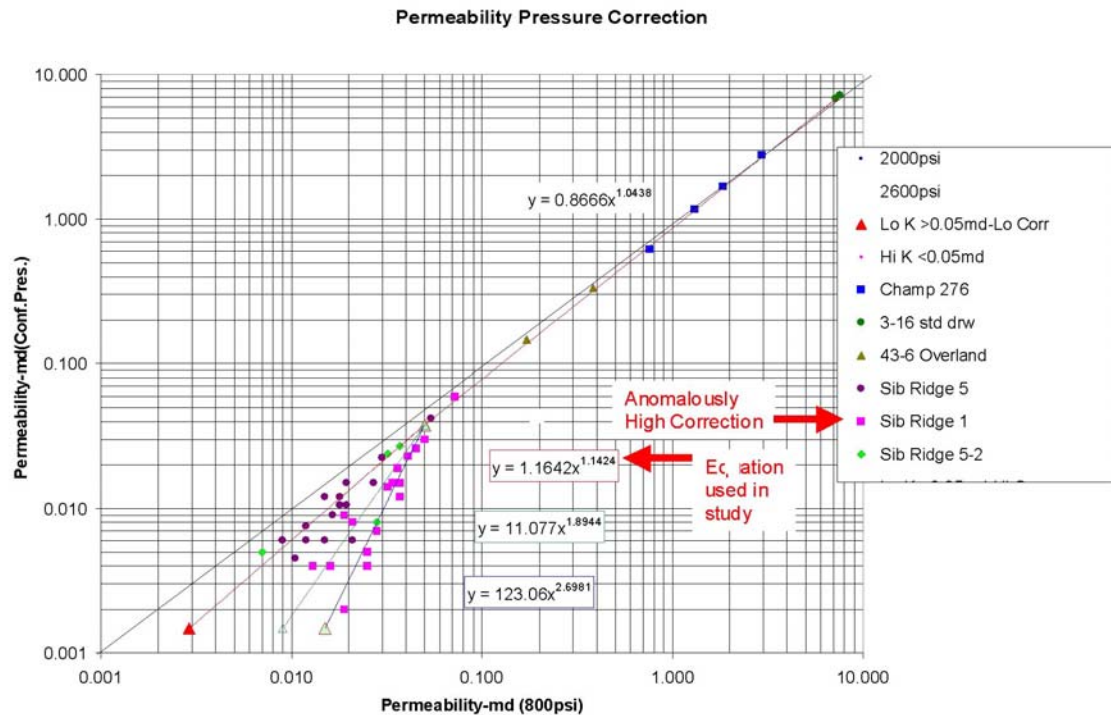


**Fig. E-2. Porosity pressure corrections  $(PHI_{nms}) = (1.155 * PHI) - 0.594$**

Due to its anomalously high permeability correction, the Siberia Ridge-1 data was considered suspect, and excluded from the analysis.

Based on this sampling, the core permeability correction is shown in fig. E-3.



$$\begin{aligned} \text{For } K > 0.05\text{md} \\ K(\text{nms}) &= 0.8666 * (K^{1.0438}) \\ \text{For } K < 0.05\text{md} \\ K(\text{nms}) &= 1.1642 * (K^{1.1424}) \end{aligned}$$

**Fig. E-3. Permeability pressure correction**

If the Siberia Ridge-1 data is valid, a higher permeability correction may be necessary. This could result in permeabilities an order of magnitude lower at the very low end of the effective permeability range (<0.02md). General core shifts were done by comparing core gamma ray or porosity to log curves, and bulk shifting appropriately.

## ***Temperature Curve***

The formation temperature is a function of the true vertical depth (TVD) as in the equation in Table E-2.

**Table E-2. Equation: formation *temperature* as a function of the TVD**

$$\text{TEMP} = 45^{\circ}\text{F} + [\text{TVD}(\text{ft}) * 0.016^{\circ}\text{F}/\text{ft}]$$

## ***Pressure Curve***

The formation pressure is a function of the true vertical depth (TVD) as in the equation in Table E-3.

**Table E-3. Equation: formation *pressure* as a function of the TVD**

$$\text{PRES} = \text{TVD}(\text{ft}) * 0.584$$

## ***Curve Normalization***

Due to the different nature of tools (cased and openhole), vintage, and calibration methods, the gamma ray curve generally has to be normalized to make direct comparisons between wells. The Almond formation has no continuous thick shales that can be used to characterize the shale point.

Moreover, thin section point counts of clay were not provided. As a result, the clean and shale points are determined by taking the 5<sup>th</sup> and 95<sup>th</sup> percentile from the cumulative frequency diagrams from the L9 pick in the overlying Lewis shale to the Almnd\_SH2 pick near the base of the section (fig. E-1). Both of these picks are present in most of the wells.

## ***Vshale – Vclay***

The Vshale was calculated (Table E-4) using the gamma ray linear (GRL) stretch between clean and shale endpoints of 20 and 130 on the normalized gamma ray curve.

**Table E-4. Equation: calculation for Vshale**

$$\text{VSHGRL} = [\text{GR}(\log) - \text{GR}(\text{clean})] / [\text{GR}(\text{shale}) - \text{GR}(\text{clean})]$$

Vclay is different from Vshale. Whereas Vshale adequately estimates the shale content of the rock, it greatly overestimates the actual clay content, which is used in most petrophysical analyses.

With the exception of very deep-water shales, even the purest shales are only 30%-50% clay with the rest of the material being lithic fragments and quartz silt. As a result, the VSHGRL curve is modified by the Steiber equation (VCLSTB) to estimate the actual clay volume.

**Table E-5. Equation: Steiber equation to estimate actual clay volume**

$$VCLSTB = (0.5 * VSHGRL) / (1.5 - VSHGRL)$$

A comparison of the two methods is shown in fig. E-4. For most reservoir sands (VSHGRL < 50%), the Steiber Vclay is roughly half the gamma ray linear Vshale.



**Fig. E-4. VSHGRL – VCLSTB**



## **Porosity**

A number of porosity techniques were attempted on the openhole logs and calibrated to core data. These techniques include:

- Neutron-density crossplot
- Density porosity
- Neutron-density sum of squares
- Neutron porosity

In every technique, it was necessary to apply a correction based on the V<sub>clay</sub> to match the core porosity data. Therefore, in this study the effective porosity is being calibrated rather than the total porosity. Of all the techniques attempted, the effective neutron-density crossplot porosity and the density porosity with variable grain density worked best.

The sand mineralogy includes varying percentages of quartz and feldspar sand grains, silica and dolomite cement and illite, kaolinite and chlorite clay (1989 Keighin et al), which result in a variable grain density across the section. The problem of the variable grain density is best addressed by the neutron-density crossplot porosity. In this method, the neutron porosity must be in limestone units.

The resultant calculation is independent of grain density. The effective porosity is used with the V<sub>clay</sub> correction, and the parameters of 2.52 g/cc clay density (mostly illite) and shale neutron of 22%, as recommended in the Gas Research Institute (2000) study.

The major problem with this technique is that due to the small hole size, an eccentralizer could not be run in most wells. This causes the neutron tool to occasionally bounce along the edge of the hole resulting in the tool standoff to be much larger (1-2 inches) than the typical 0.25-0.50 inches (Lesley Evans and Leif Colson). This causes the tool to read high porosity locally (fig. E-5), which is difficult to identify except by matching to other porosity techniques in the same hole or interval to interval comparison with nearby wells.

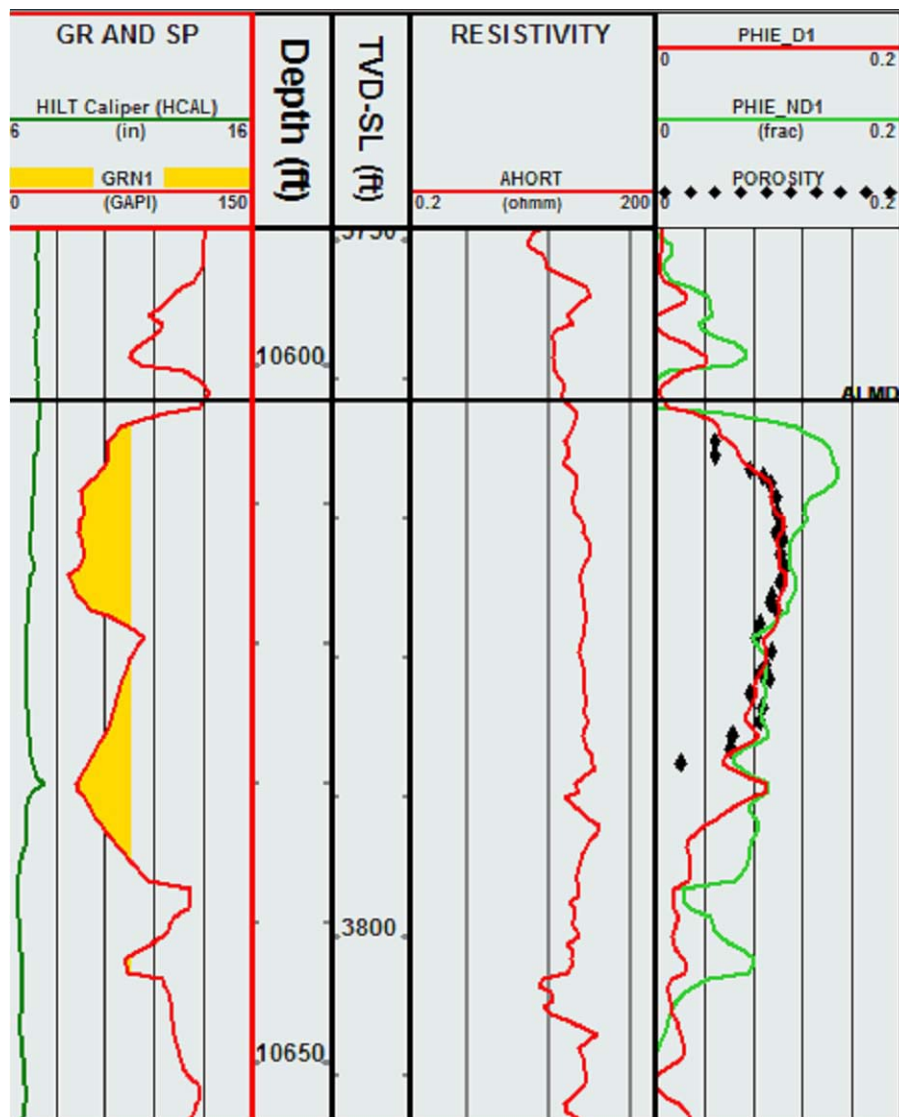


*Fig. E-5. Erratic neutron effects on porosity.*

In cases where the neutron is suspect, the density method is used. Due to complex mineralogy, the grain densities are variable, and it is necessary to alter the grain density based on stratigraphic interval (fig. E-6). In low porosity, nonreservoir rocks, the grain density normally reads high due to the dolomite cement (2.78 g/cc).

This will artificially weight the grain density higher than that found in productive sands. Therefore, only grain densities associated with reservoir quality sands (porosity  $\geq 8\%$ ) are used in the analysis.

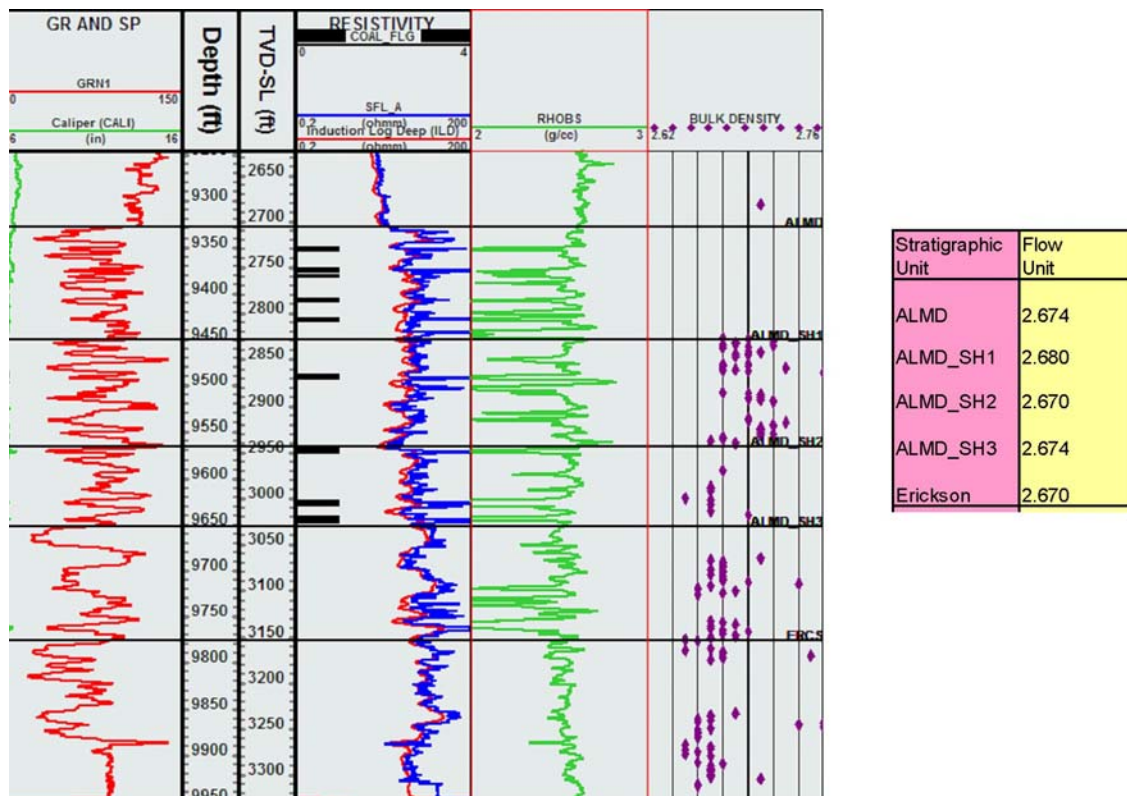


**Fig. E-6. Grain density**

Another problem is that there appears to be a minor gas effect in some of the cleaner sands in some wells. Here, a first pass flushed zone water saturation ( $S_{xo}$ ) was made using the shallow resistivity, and the Archie equation.

In general, the rocks are so tight, that capillary forces pull the mud filtrate into the rock, which displaces most of the gas, leaving some residual gas is left behind. In most rocks, this minor gas effect results in only a 0-0.5 porosity unit correction. The total density porosity is shown in Table E-6.

**Table E-6. Equation: total density porosity correction**

PHIT =	$\frac{[\text{DEN}(\text{matrix}) - \text{DEN}(\text{log})]}{[\text{DEN}(\text{matrix}) - ((\text{Sxo} * \text{DEN}(\text{fluid})) + ((1 - \text{Sxo}) * \text{DEN}(\text{gas})))]}$
--------	--

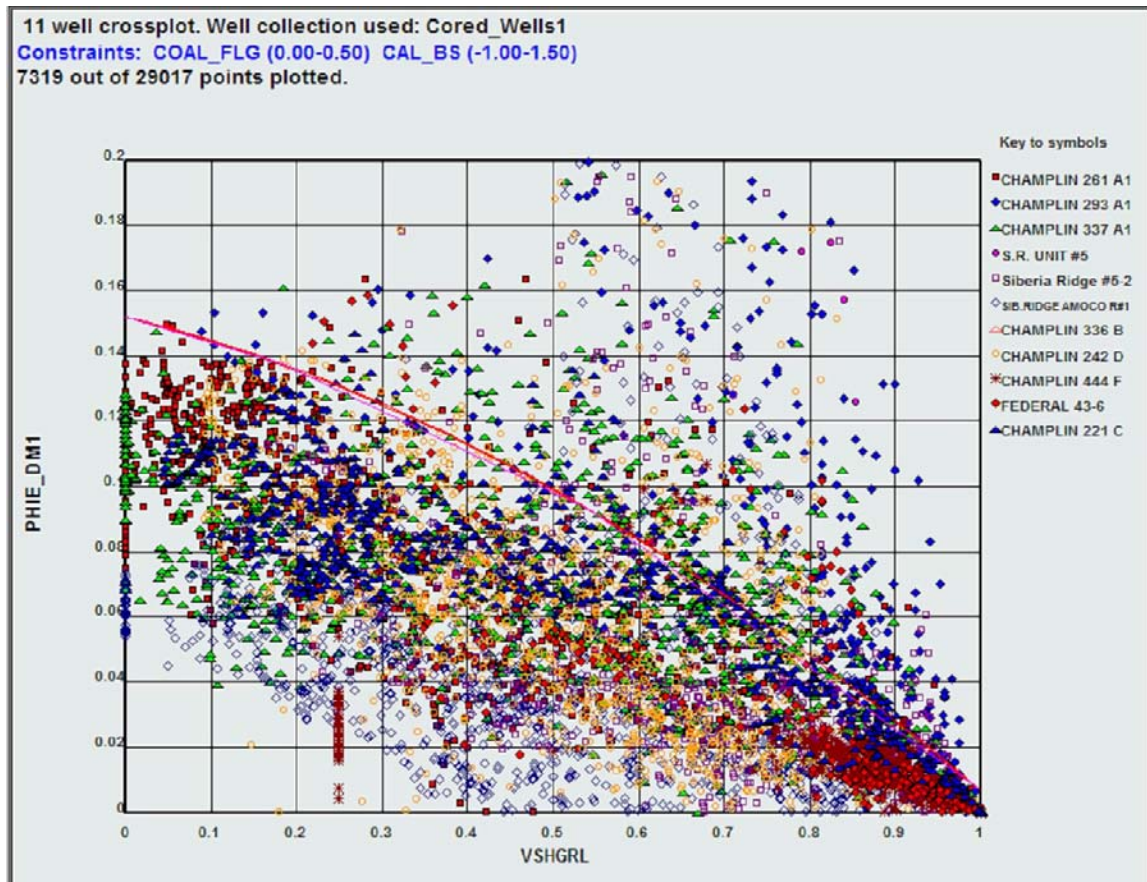
The effective density porosity (PHIE) is weighted by the Vclay, as shown in the equation in Table E-7.

**Table E-7. Equation: PHIE weighted by Vclay**

<p>PHIE = PHIT * (1 - Vclay)</p> <p>DEN(mat) = 2.670-2.680 g/cc (varies by interval; fig. E-6)</p> <p>DEN(log) = values from the density curve</p> <p>DEN(fluid) = 1.00 g/cc (fresh water mud filtrate)</p> <p>DEN(gas) = 0.15 g/cc (gas)</p> <p>Sxo = near bore water saturation due to filtrate invasion</p> <p>Vclay = Volume of clay (Steiber method)</p>
---

## Vshale-Porosity Transform

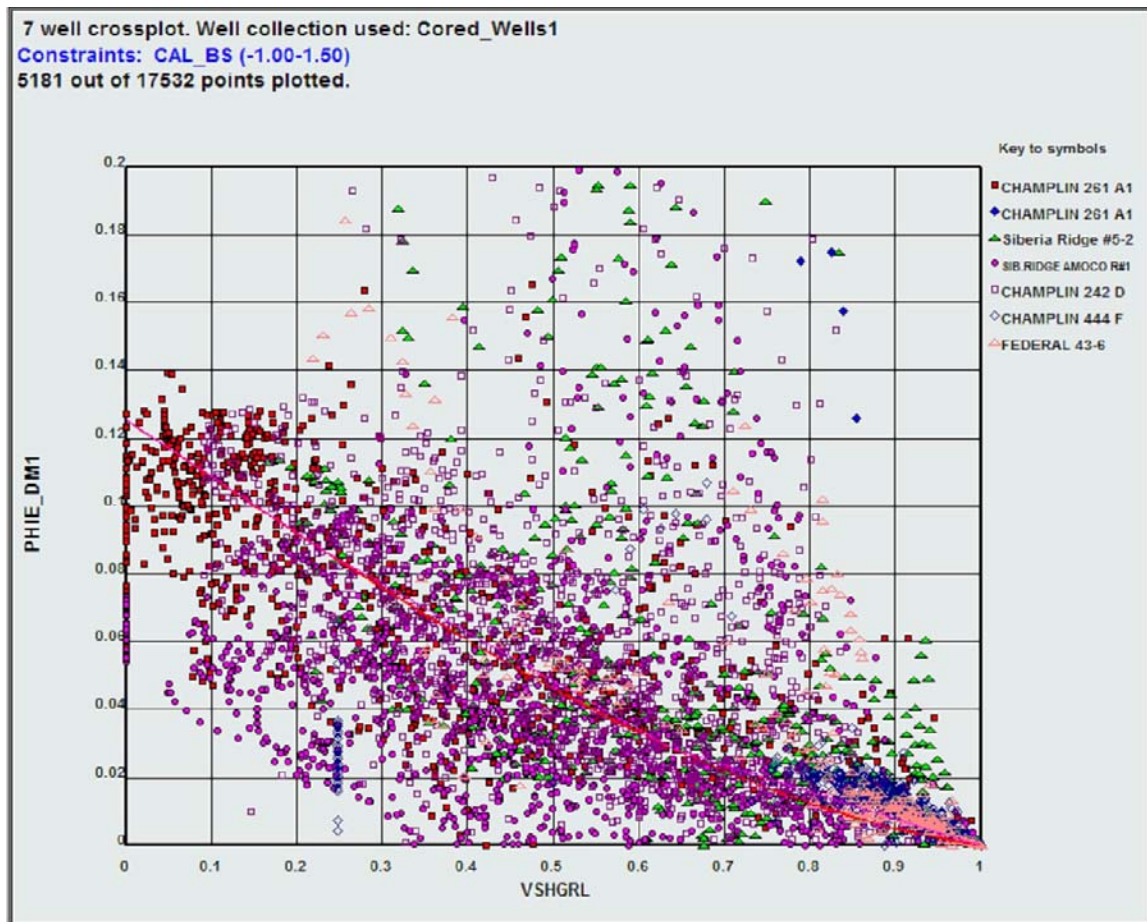
In zones of high washout neither the density nor the neutron logs adequately read the formation porosity. In these intervals the porosity is calibrated to the Vshale curve. Three transforms are used. The first brackets the maximum porosity for a given Vshale value (fig. E-7).



$$PHI_{max} = 0.1519 + (-0.621 \cdot VSHGRL) + (-0.8868 \cdot (VSHGRL^2)) + (0.005872 \cdot (VSHGRL^3))$$

*Fig. E-7. VSHGRL – PHE PHI<sub>max</sub>*

The second is a transform through the middle of the data trend (fig. E-8).



$$PHI_{mean} = 0.1256 + (-0.1686 * VSHGRL) + (-0.003277 * (VSHGRL^2)) + (0.04610 * (VSHGRL^3))$$

**Fig. E-8. VSH – PHIE PHI<sub>mean</sub>**



The third transform is the average of the maximum and mean Vshale-derived porosity as shown in Table E-8.

**Table E-8. Equation: average of maximum & mean Vshale-derived porosity**

$$PHI_{avg} = (PHI_{max} + PHI_{mean}) / 2$$

Where washout occurs, the trend that best mimics the data in good holes above and below the washed out section is spliced into the curve. In general, the shales and siltstones match the  $PHI_{mean}$  curve. The reservoir quality sands match the  $PHI_{avg}$  curve. If the hole is good, and the porosity curve exceeds the  $PHI_{max}$  calculation, then this usually indicates that the rock is a coal or the log curves are in need of shifting or editing.

Effective porosity in most reservoir quality sands ranges 8%-12%, and rarely exceeds 14%. Results for all cored wells are shown in figs. E-9 through E-16.

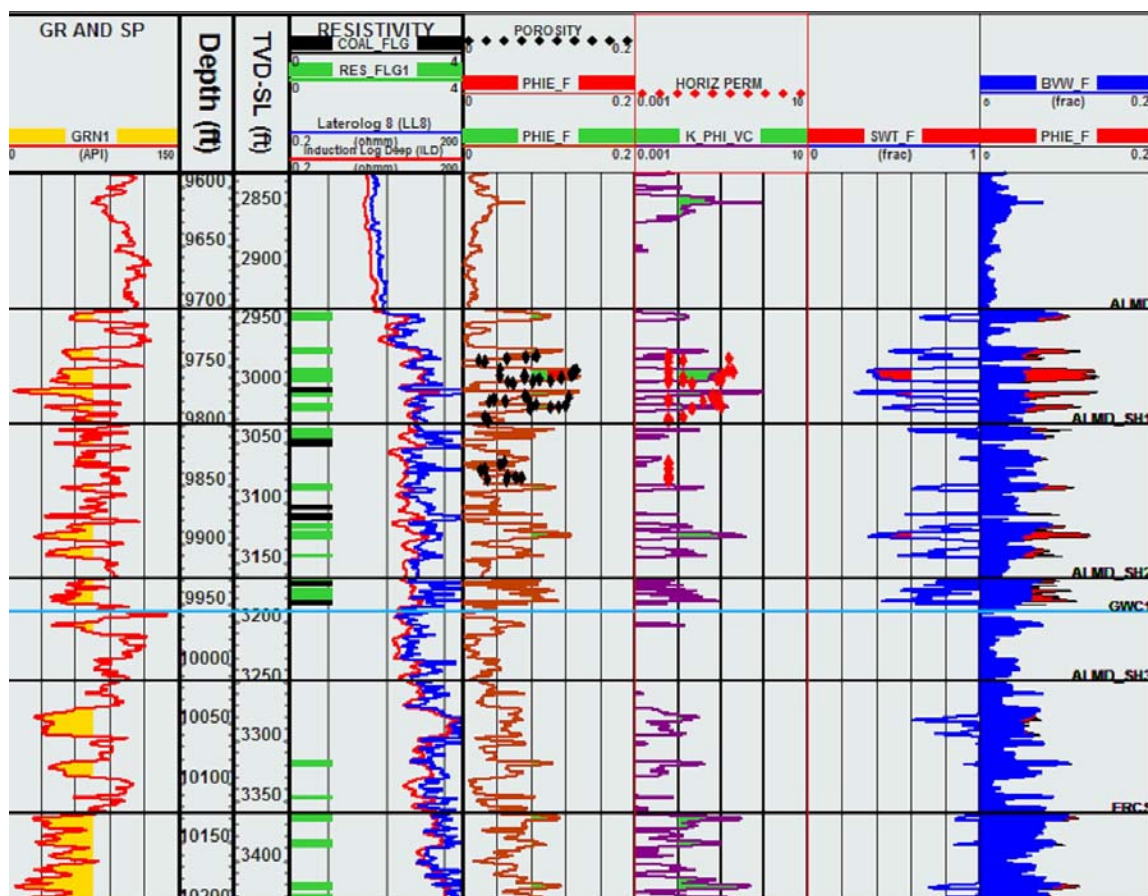


**Fig. E-9. Champlin 337 A1**

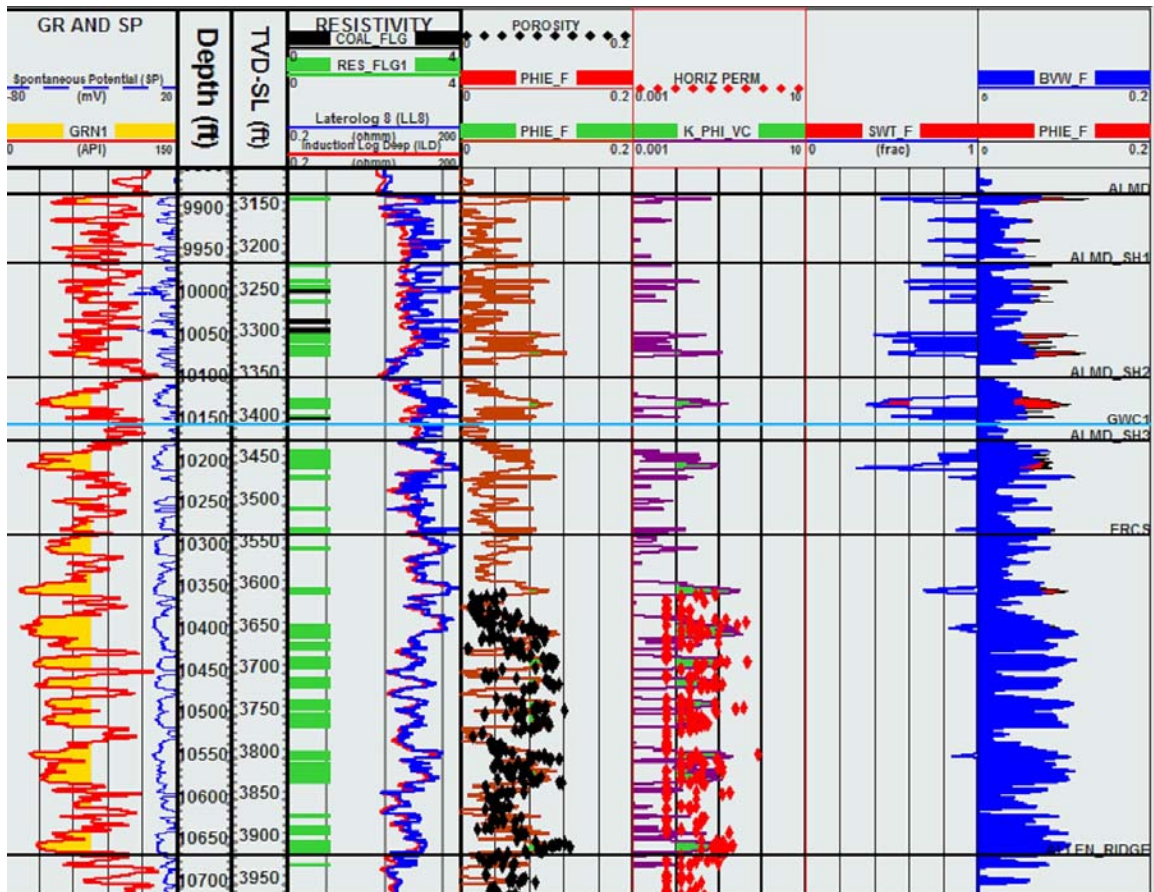


Fig. E-10. Champlin 261 A1



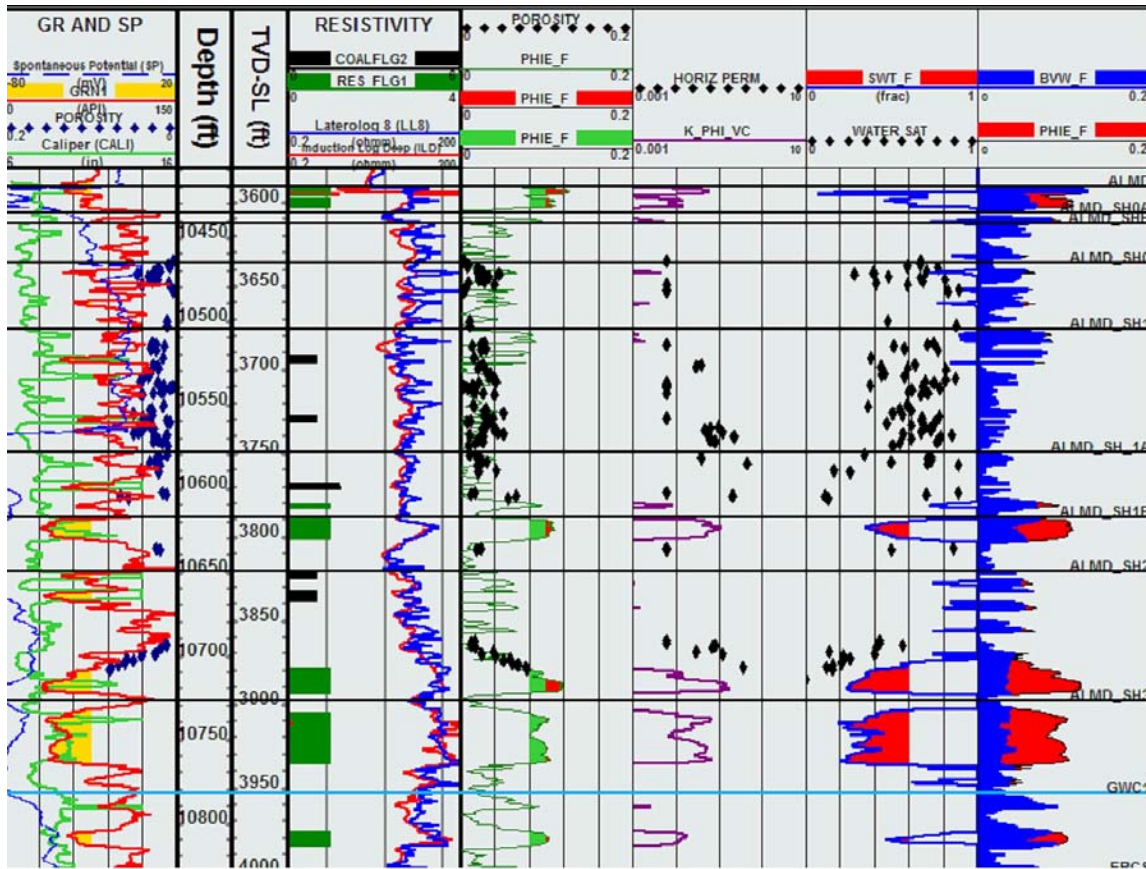


Fig. E-11. Champlin 293 A1

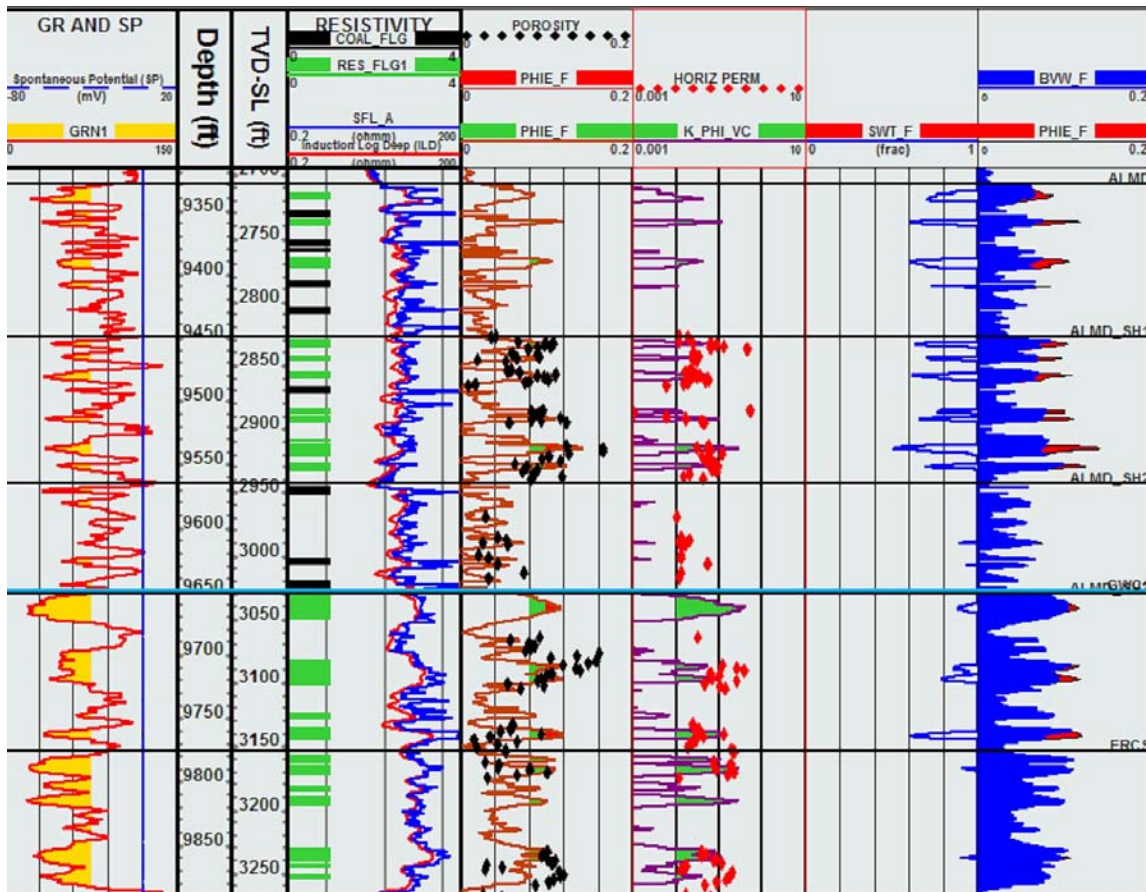


Fig. E-12. Champlin 336 B

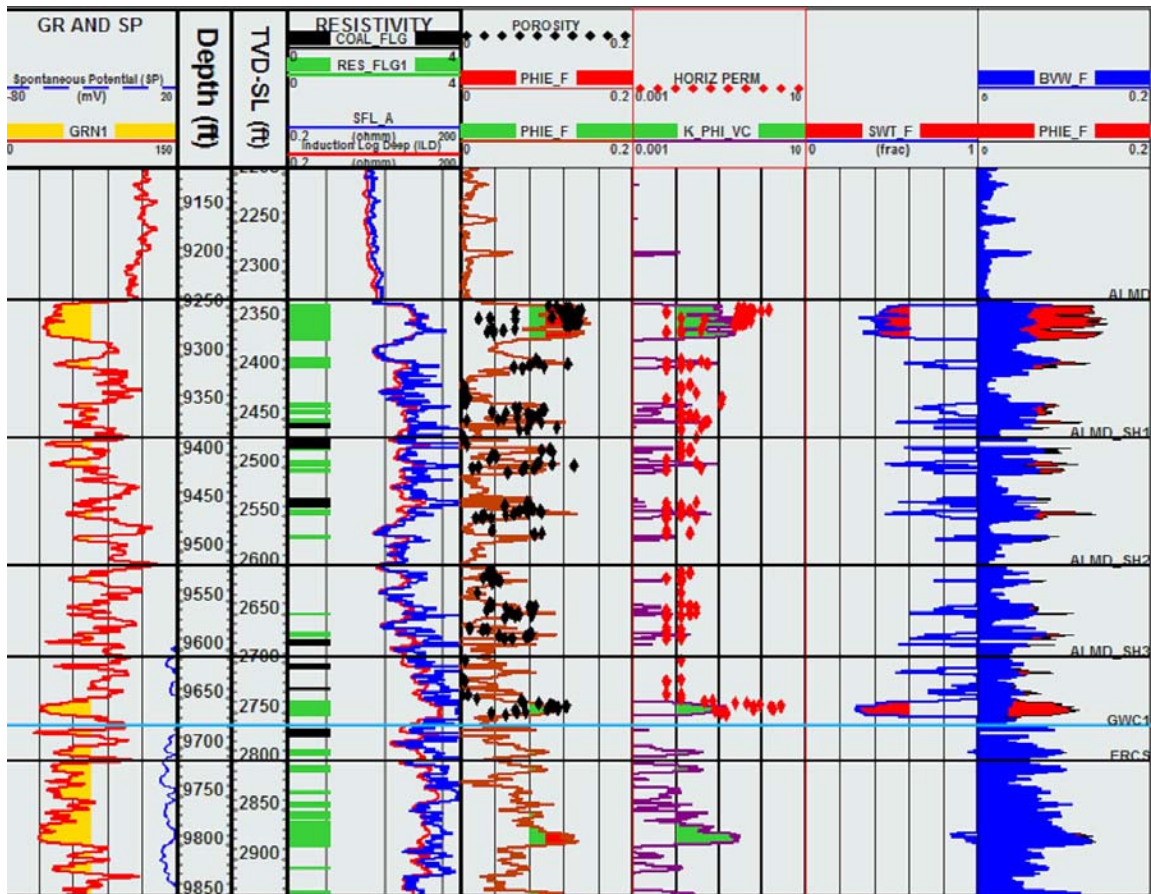


Fig. E-13. Champlin 242 D



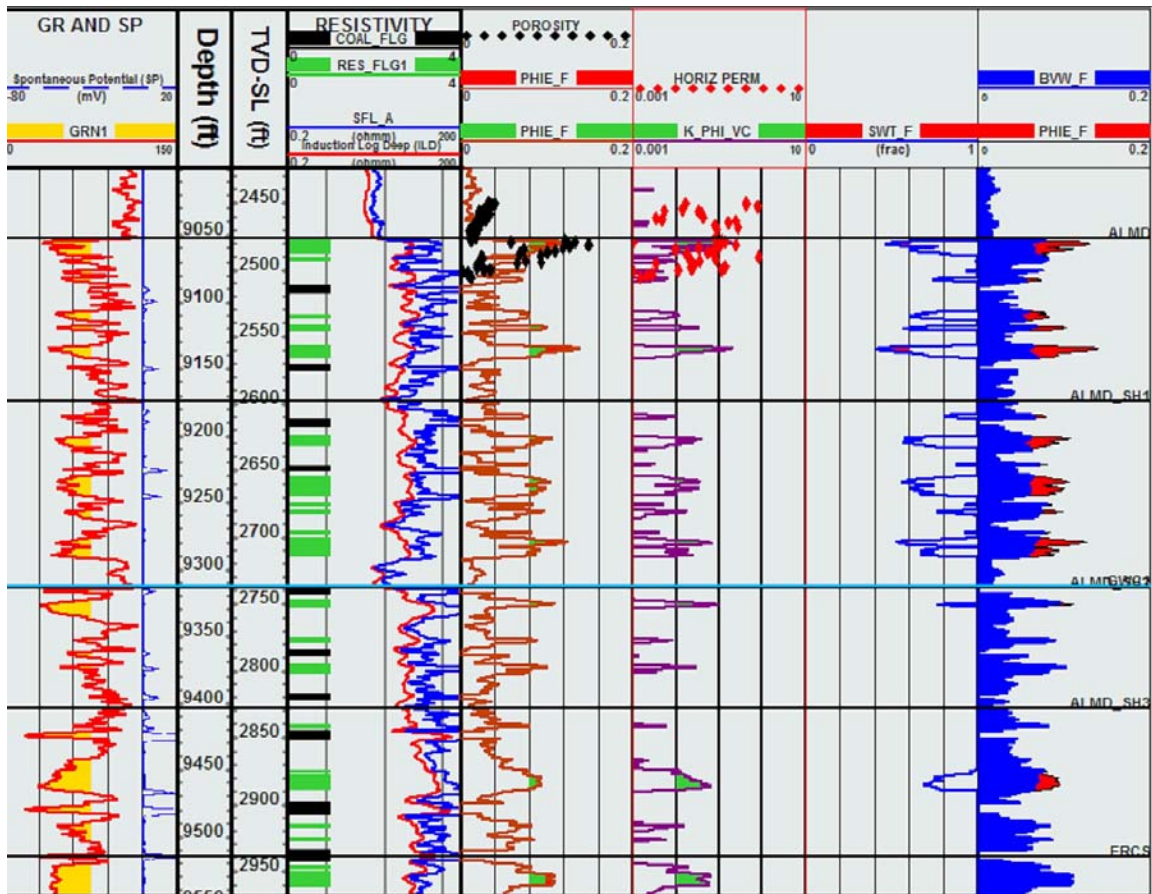


Fig. 14. Champlin 444 F

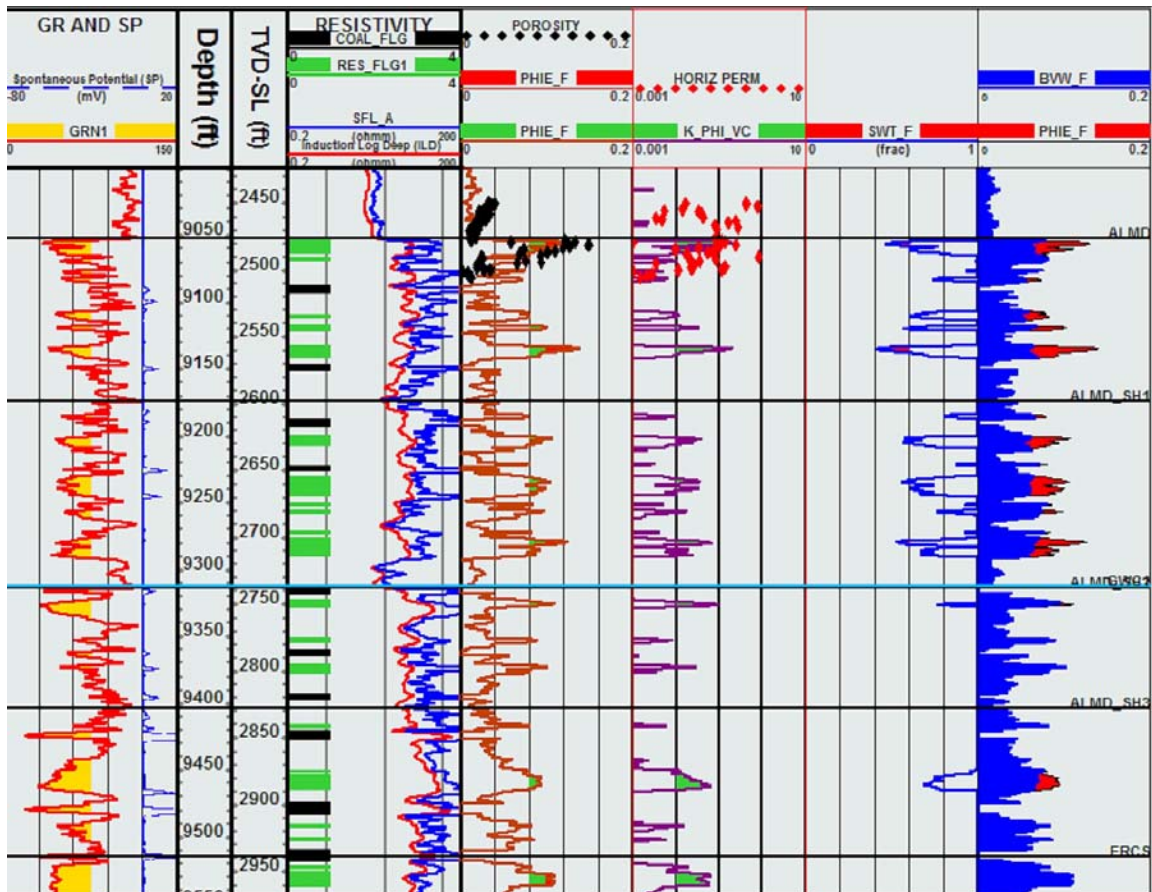


Fig. E-15. Federal 43-6

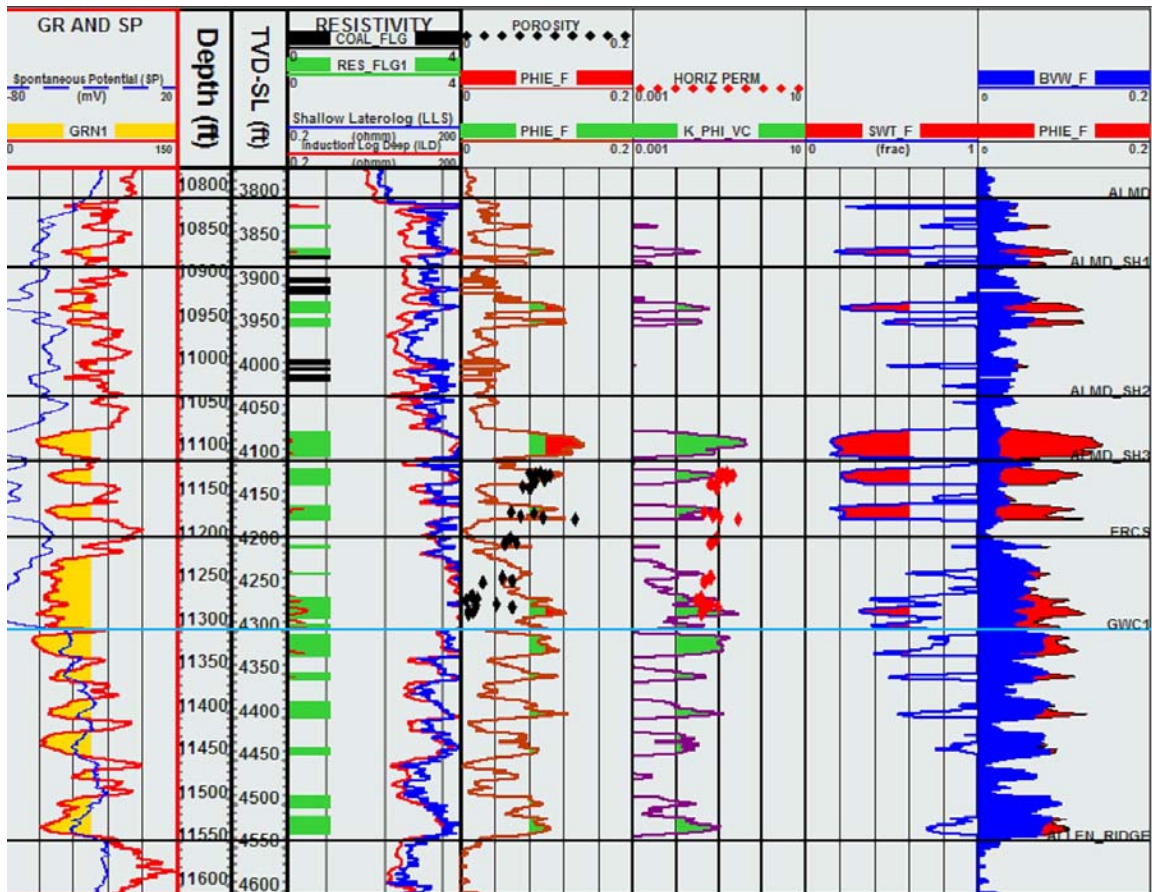


Fig. E-16. Champlin 221 C

## Cased Hole Pulsed Neutron Logs

Once the openhole logs were run for porosity, the cased hole pulsed neutron logs were calibrated. Good openhole and TDT logs were found together in wells BP Frewin Unit 19-9, Amoco Coal Bank 2-7, and Champlin 444.

In general, the cased hole pulsed neutron porosity (TPHI) does a good job of matching the openhole neutron porosity log, so the total porosity provided by the service company needs to be corrected for clay, and scaled to the openhole porosity (fig. E-17), as shown in the equations in Table E-9.

**Table E-9**

**Equation: Correction for clay and openhole porosity**

$$\text{TPHIE} = \text{TPHI} \cdot (1 - \text{VCLSTB})$$

$$\text{PHIE\_TDT} = (-0.1486) + (8.1578 \cdot \text{TPHIE}) + (-138.1 \cdot (\text{TPHIE}^2)) + (826.34 \cdot (\text{TPHIE}^3))$$

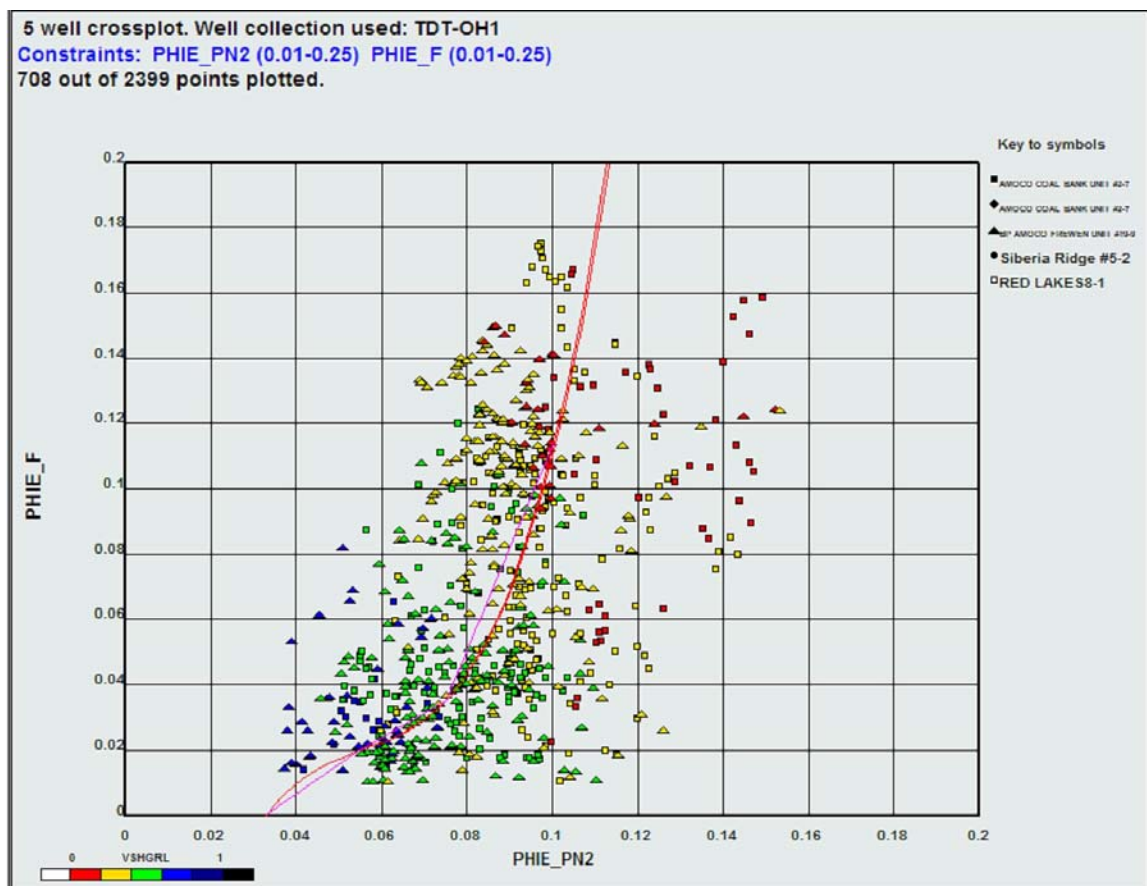
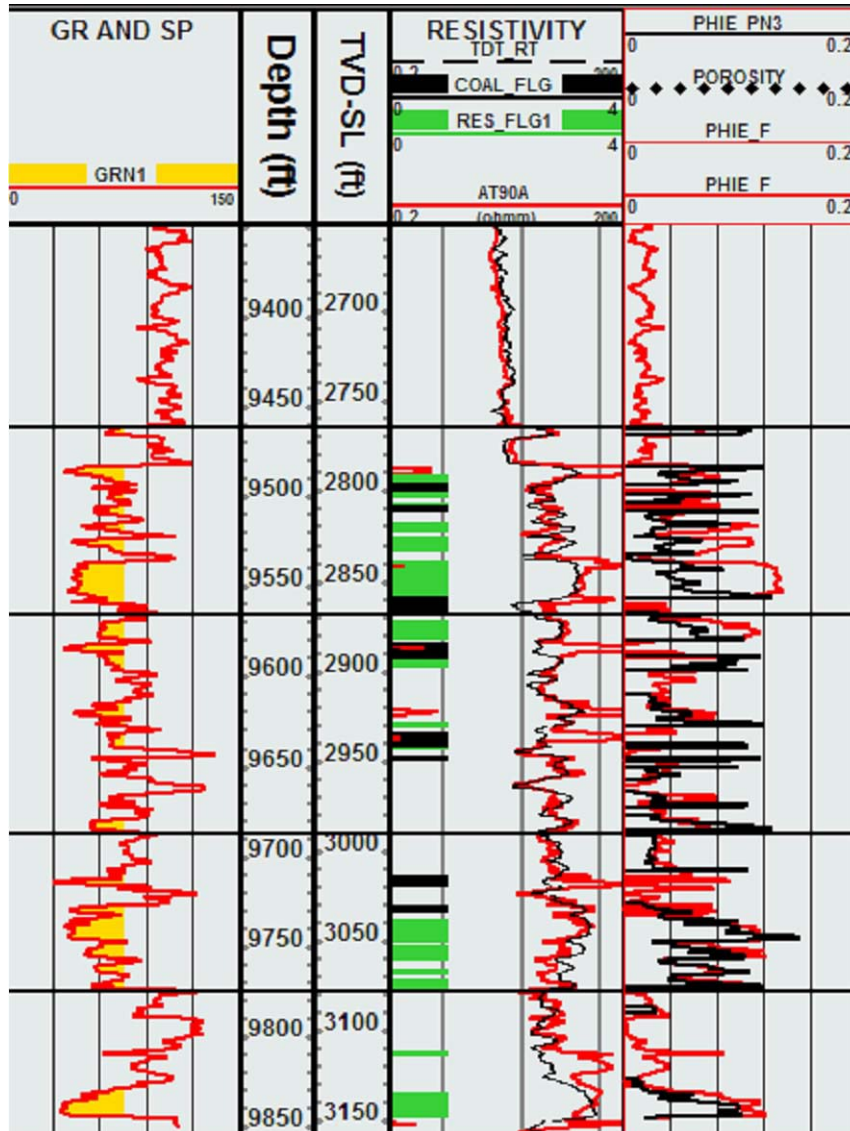


**Fig. E-17. TDT PHIE-PHIE\_PN2**



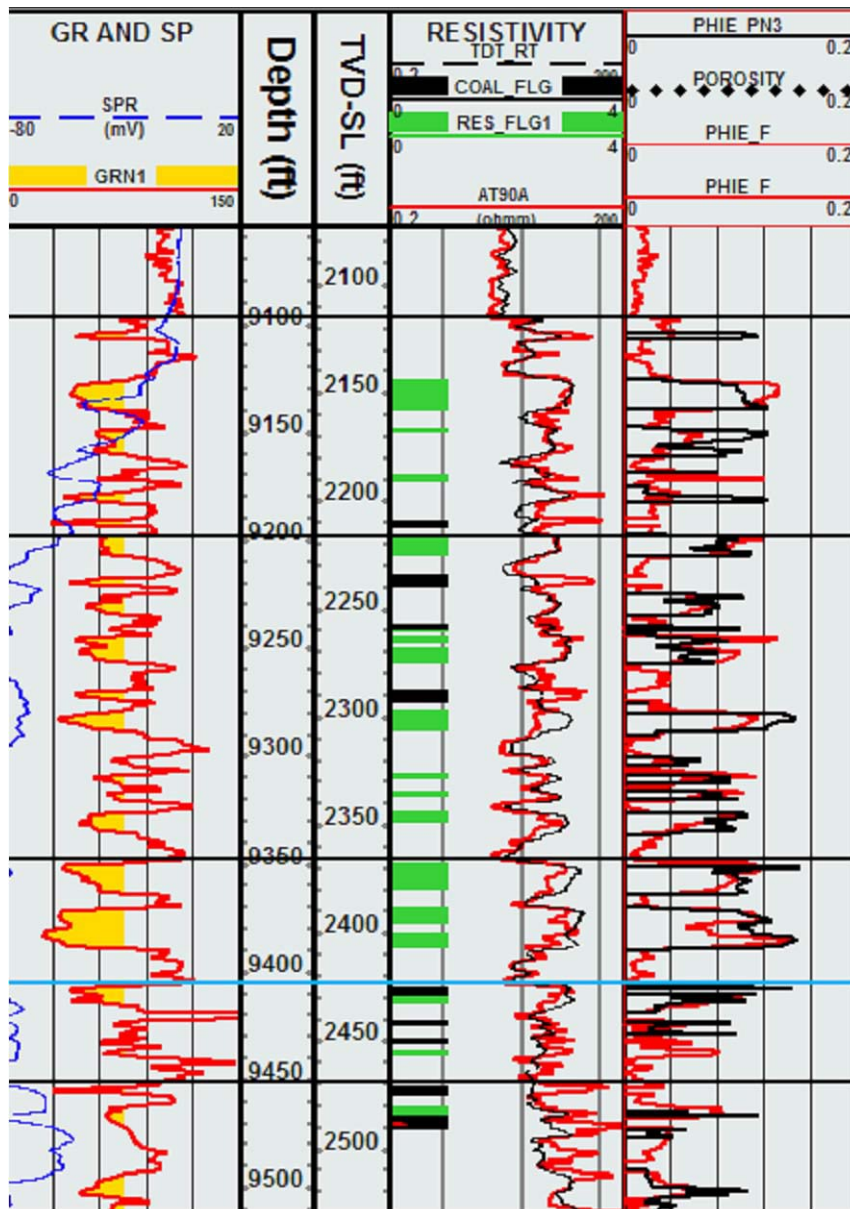
Comparisons of the openhole and cased hole porosities are shown in figs. E-18 through E-20. When compared to nearby wells with good openhole logs, only about half of the cased hole logs were deemed useful for property distribution.



**BP Frewin Unit 19-9 well:** Although there are some discrepancies, the cased hole porosity (PHIE\_PN3) does a good job of matching the openhole porosity (PHIE\_F) in most of the reservoir quality sands (PHIE>0.08).

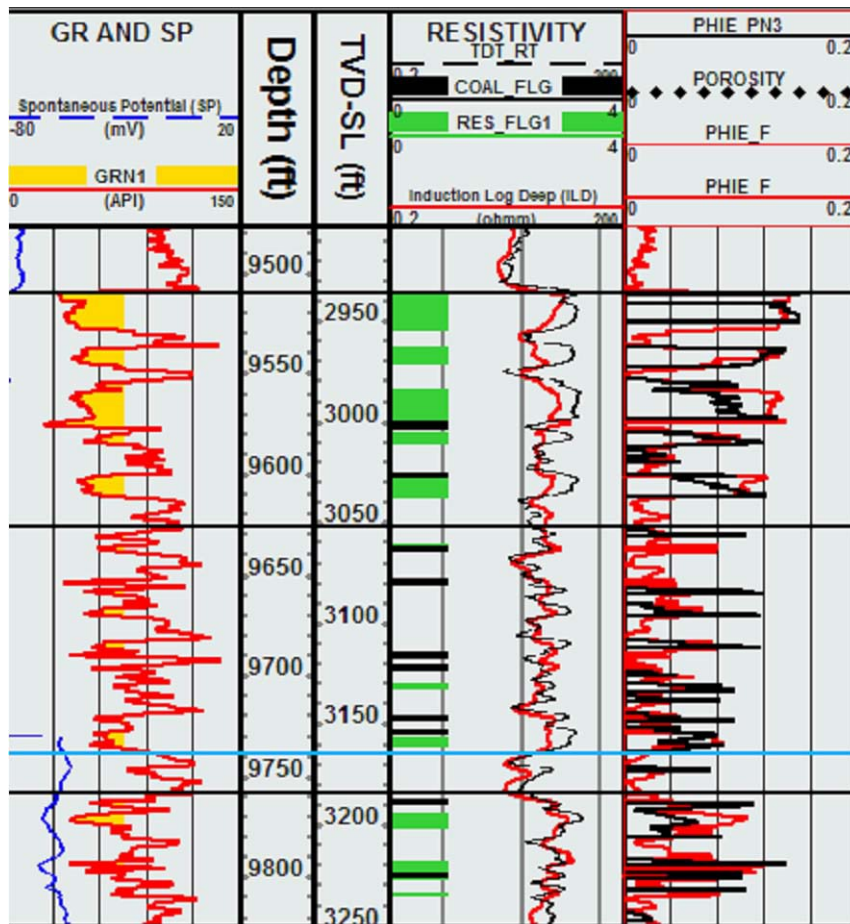
*Fig. E-18. BP Frewin Unit 19-9*





**Amoco Coal Bank 2-7 well:** Although there are some discrepancies, the cased hole porosity (PHIE\_PN3) does a good job of matching the openhole porosity (PHIE\_F) in most of the reservoir quality sands (PHIE>0.08).

**Fig. E-19. Amoco Coal Bank 2-7**



**Champlin 444 well:** Although there are some discrepancies, the cased hole porosity (PHIE\_PN3) does a good job of matching the openhole porosity (PHIE\_F) in most of the reservoir quality sands (PHIE > 0.08).

*Fig. E-20. Champlin 444*

## Coal Flag

On both the neutron and density curves, the coals read as very high porosity, but have a low gamma ray response similar to pay sands. In order not to misidentify these intervals as reservoir sands, a coal flag was made based on the conditions in Table E-10.

**Table E-10. Equation: conditions used to flag coal**

$\begin{aligned} & \text{RHOB} < 2.3 \ \& \ \text{VSHGR} < 0.5 \ \& \ \text{NPHI} > 0.45 \ \text{ or} \\ & \text{RHOB} < 2.3 \ \& \ \text{VSHGR} < 0.5 \ \text{ (if neutron curve is poor or missing)} \\ & \text{NPHI} > 0.45 \ \& \ \text{VSHGR} < 0.5 \ \text{ (if density curve is poor or missing)} \end{aligned}$
---

For TDT curves the conditions in Table E-11 are used to flag coal.

**Table E-11. Equation: conditions used to flag coal for TDT curves**

$\text{TPHI} > 0.25 \ \& \ \text{VSHGR} < 0.5$
--

In all cases, wells are compared to other nearby wells to verify the interval is coal rather than washed out sand.

## Permeability

Due to the ambiguity of the in situ pressure correction, only core values run at 2,000-2,600 psi confining stress were used for the permeability model. Since there is not a single tight porosity-permeability trend a number of algorithms were attempted.

The first three algorithms (Table E-12) are based on a high, medium and low, direct porosity-permeability transform from the good core data (fig. E-21).

**Table E-12. K\_PHI algorithms**

$$K\_PHI\_HI = 0.0000006 * (2.714^{(116.94 * PHIE)})$$

$$K\_PHI\_MD = 0.0000008 * (2.714^{(106.27 * PHIE)})$$

$$K\_PHI\_LO = 0.000002 * (2.714^{(92.103 * PHIE)})$$

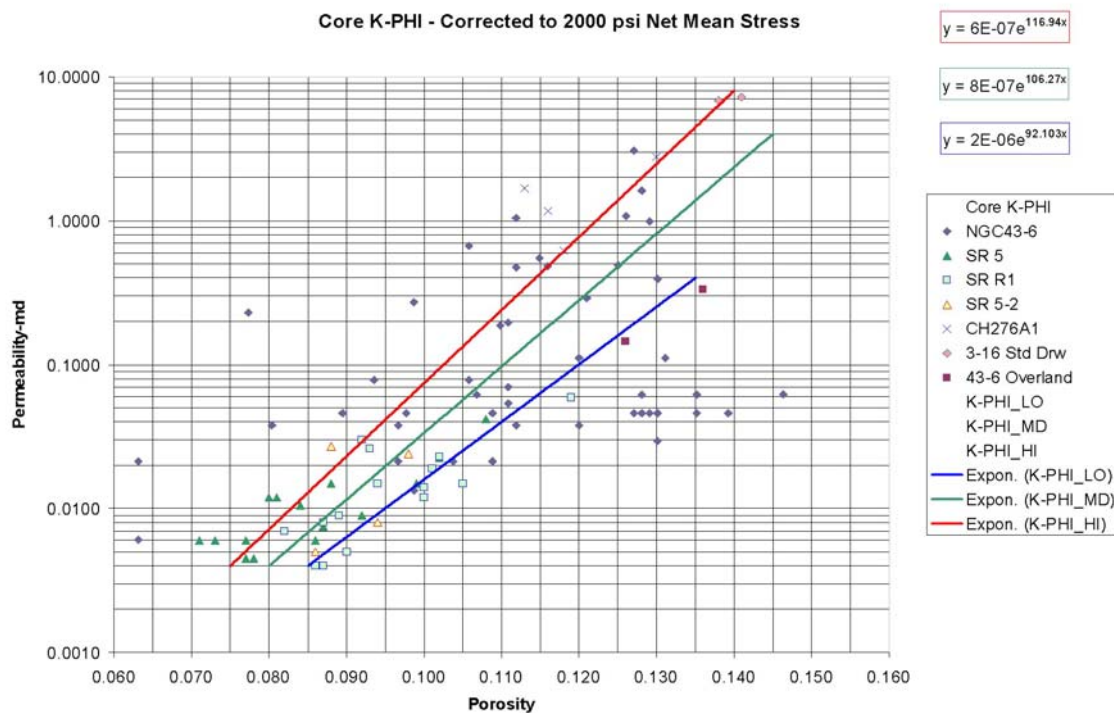


**Fig. E-21. K-PHI (@2000 psi)**

Another technique is a modified Timur-Coates equation (K\_PHI\_VC), which uses both the effective porosity and Vclay (Table E-13).

**Table E-13. Timur-Coates algorithms**

$$K\_PHI\_VC = (((PHIE/0.12)^{4.0}) * ((1.06/(VCLSTB+0.06)) - 1)^2) * 0.002$$

Of the four techniques, the modified Timur-Coates equation is the best fit with the core data (figs. E-22 through E-24).

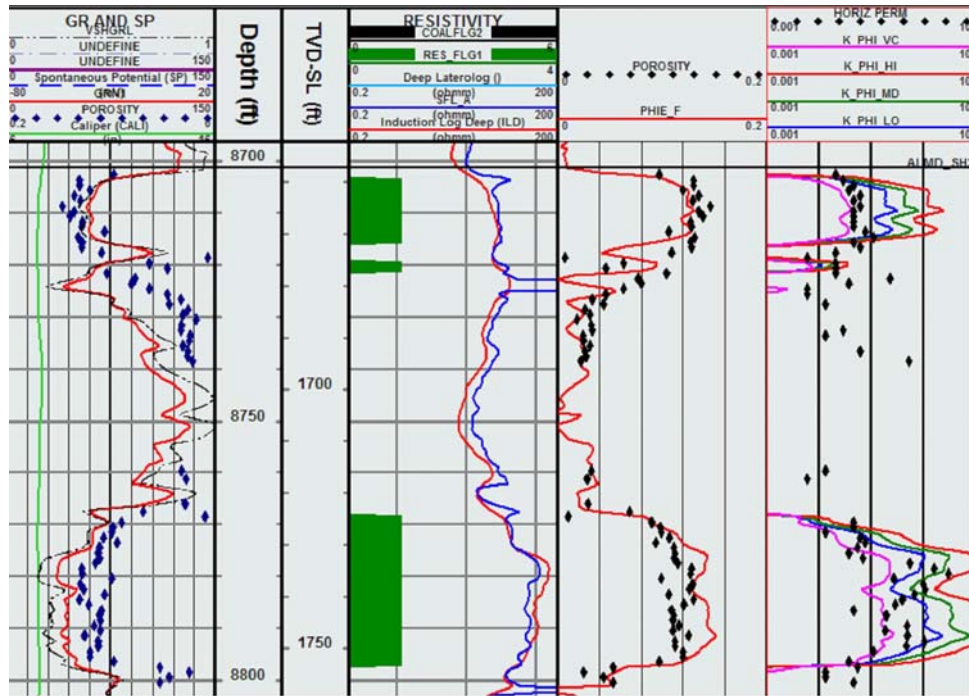


Fig. E-22. K-PHI: Federal 43-6

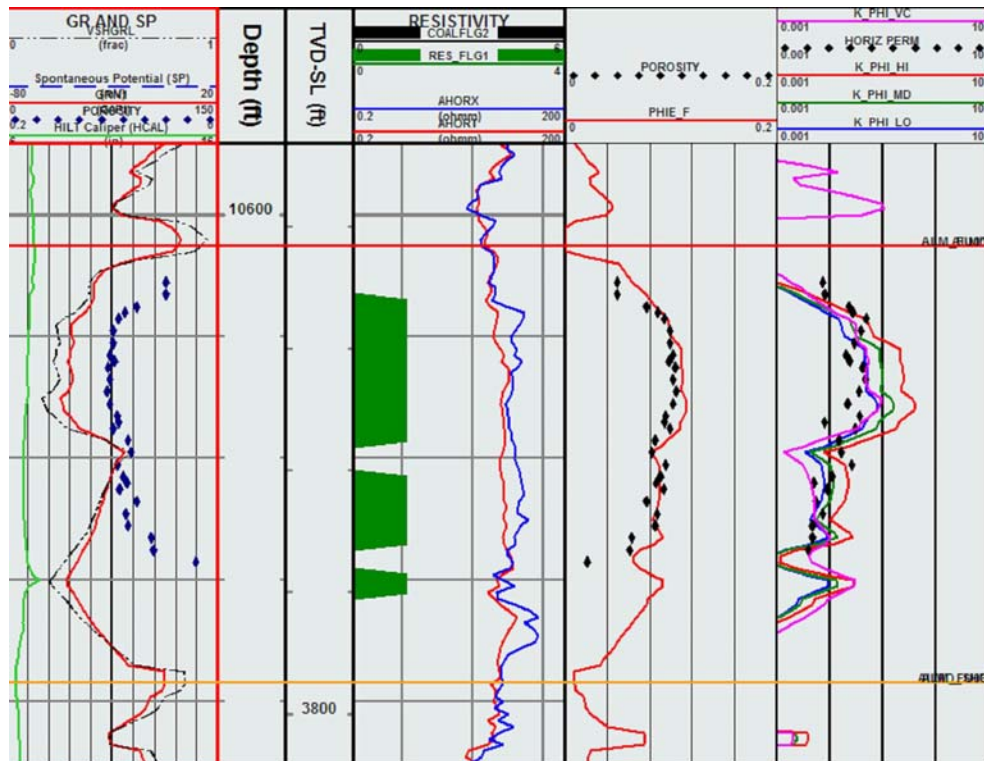
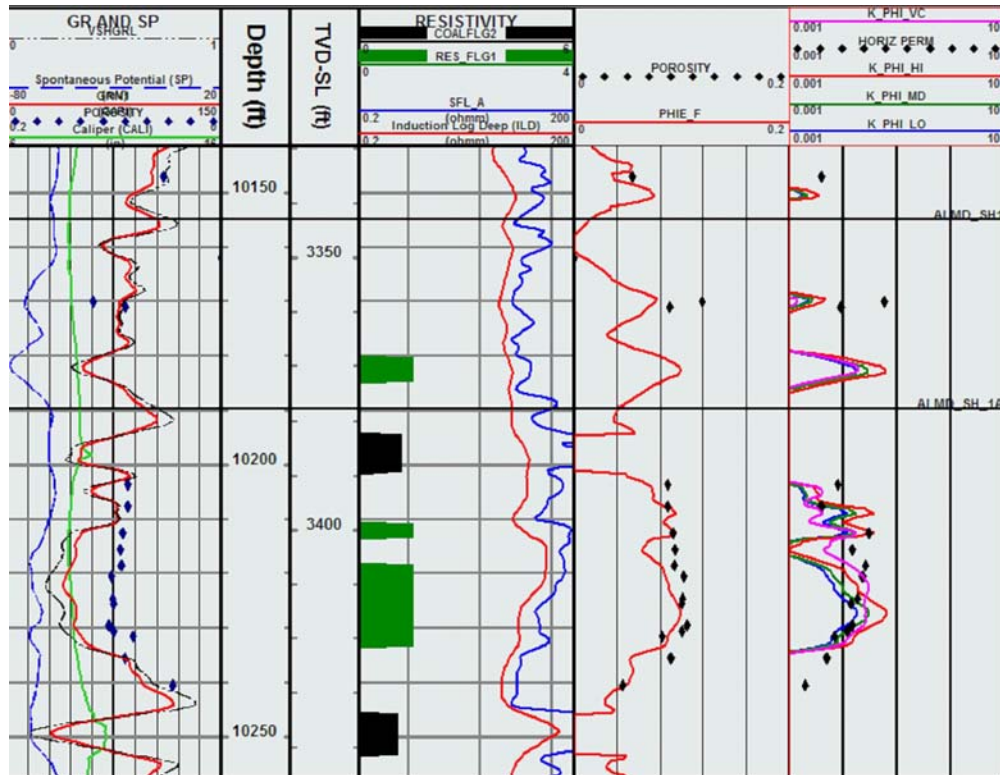


Fig. E-23. K-PHI: Siberia Ridge 5-2



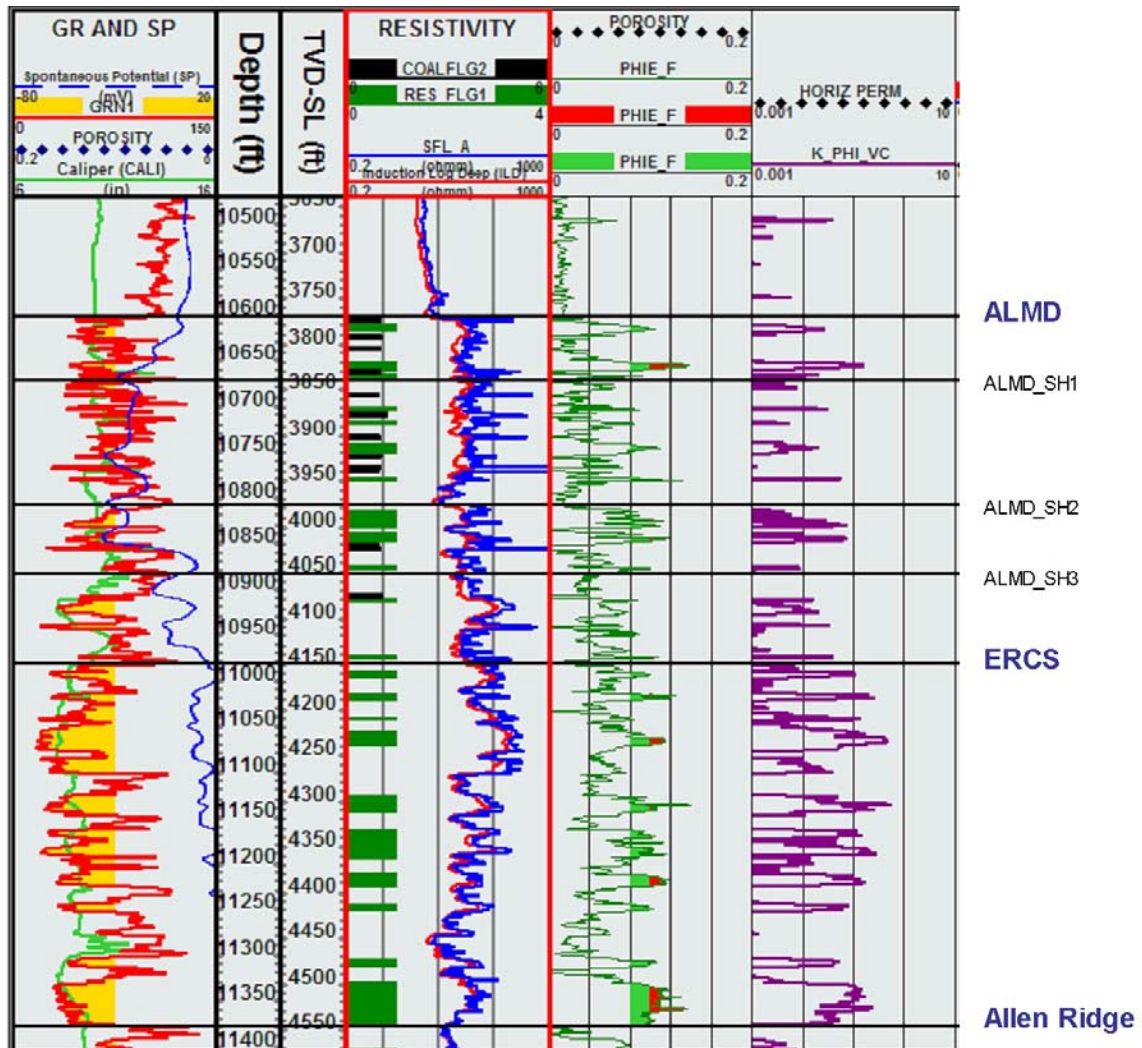


**Fig. E-24. K-PHI: Siberia Ridge R#1**

## Water Resistivity

Water samples show that the water salinity is variable within the stratigraphic section. Water in the aquifer is fresher than the formation water in the gas zone. This is also observed in the logs. In most wells, zones calculated to be gas-bearing in the Lower Almond and Ericson sands flow very fresh water.

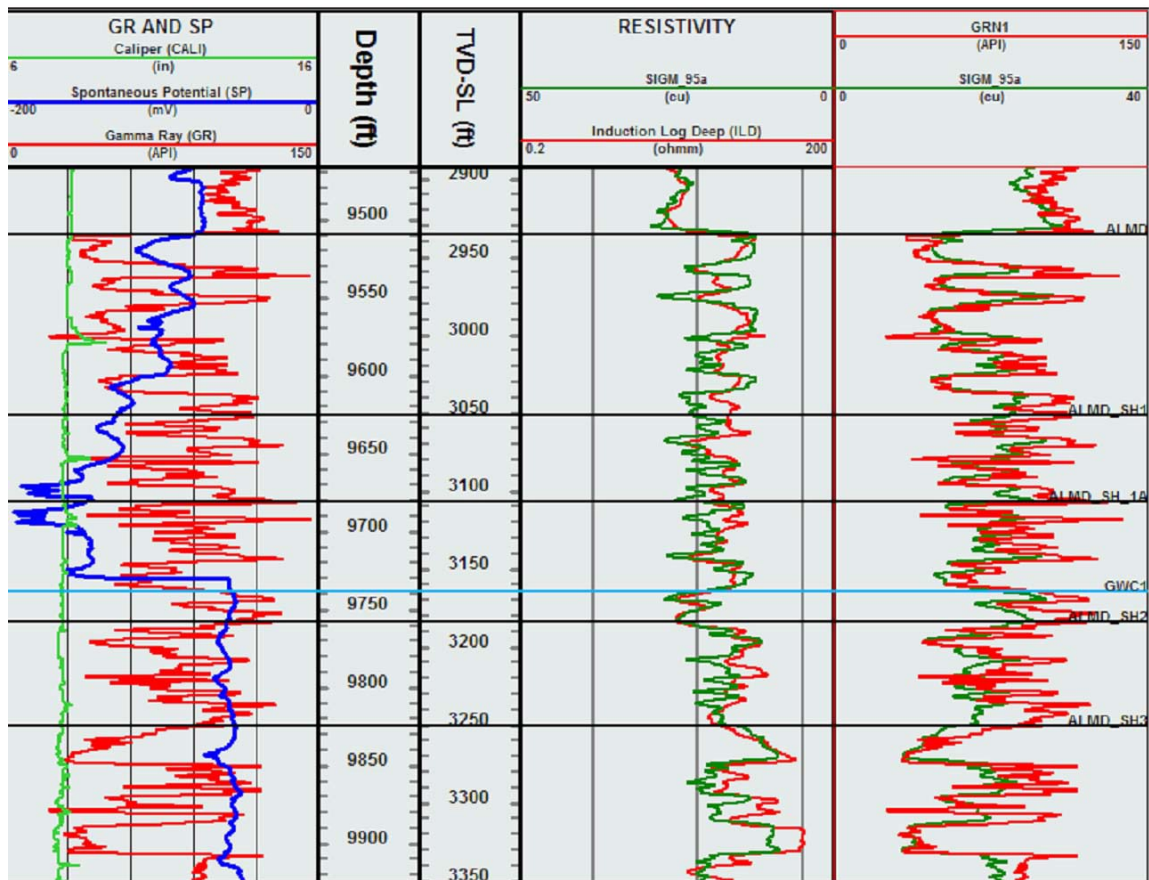
As a result, the main petrophysical problem in the reservoir is that standard water saturation calculations on both openhole and cased hole logs cannot distinguish between gas and the very fresh water in the aquifer (figs. E-25 and E-26). Water samples collected from the Almond reservoir have salinities of 15,000 to 3,000 ppm NaCl, which corresponds to resistivities ranging 0.46 to 1.98 ohm-m at 68°F.



Aquifer water is so fresh (<5,000 ppm NaCl) that it is difficult to distinguish from gas-bearing intervals. Most gas comes from the upper and middle Almond. Although the porous and permeable Ericson has high resistivity, it only produces water. Therefore, this study used water chemistry, fluids and logs in Upper and Middle Almond to calibrate  $R_w$  in gas zone, and the Ericson to calibrate  $R_w$  in the aquifer.

**Fig. E-25. Primary petrophysical challenge**

## Champlin 444



PNL sigma curve generally matches GR or deep resistivity curves, but due to fresh aquifer water (<5,000ppm NaCl), cannot distinguish gas from water.  
The sigma curve can be used as a sand/shale indicator or calibrated to deep resistivity.

**Fig. E-26. Cased hole pulsed neutron**



Based on collected water analyses and water saturation modeling, the aquifer water resistivity is presumed to be 1.74 ohm-m at 68°F (0.56 @ 200°F), or 3,500 ppm NaCl.

This corresponds to the lowest known water salinity sample collected in the field. Pickett plots (fig. E-27) show most water producing sands will calculate wet (>50% SW).

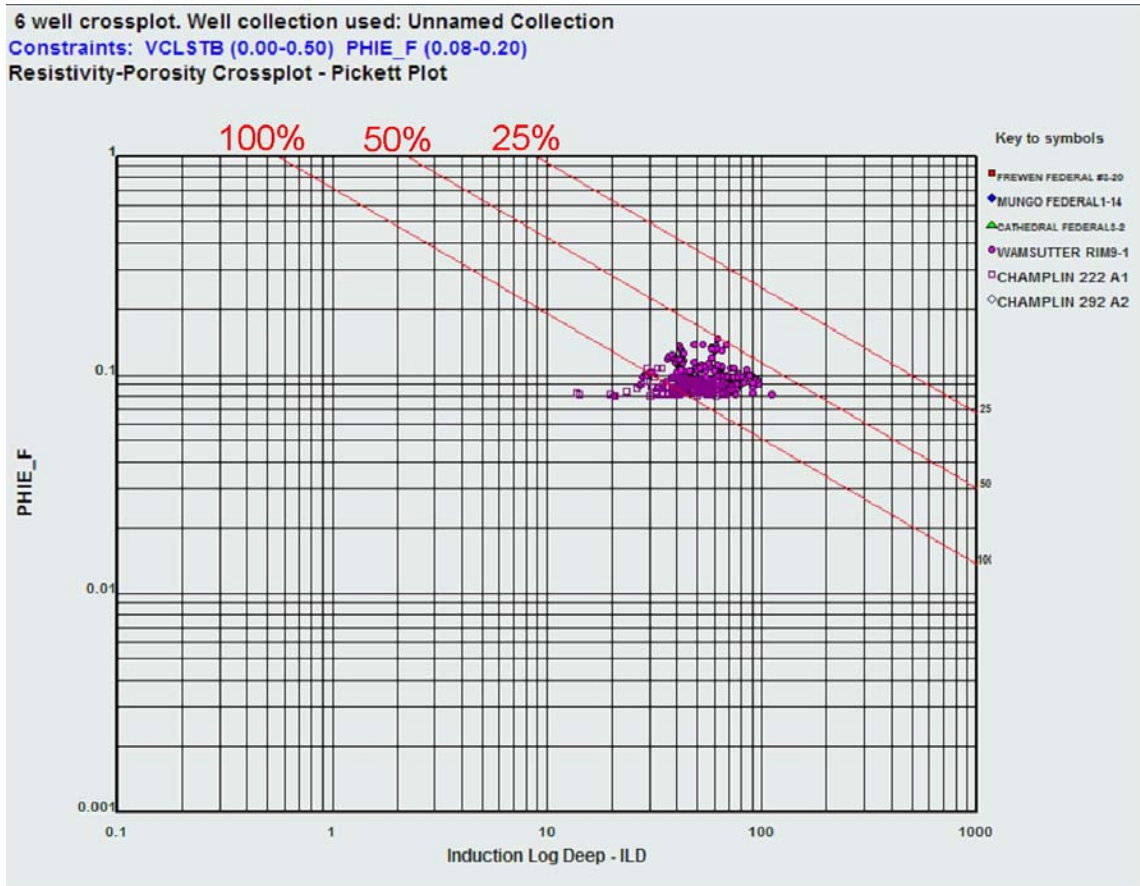


**Fig. E-27. Pickett plot aquifer –  $R_w = 1.74$  @ 68F**

On the other hand, even the known gas-bearing zones calculate wet on Pickett plots (fig. E-28) and logs with these values (fig. E-29).

Therefore, the water in the gas-bearing sands must have a higher salinity. Based on capillary pressure curves that show that water saturation in productive sands range 32%-67%, the water salinity should be 13,000 ppm NaCl, which is 0.46 ohm-m at 68°F (0.17 @ 200°F).

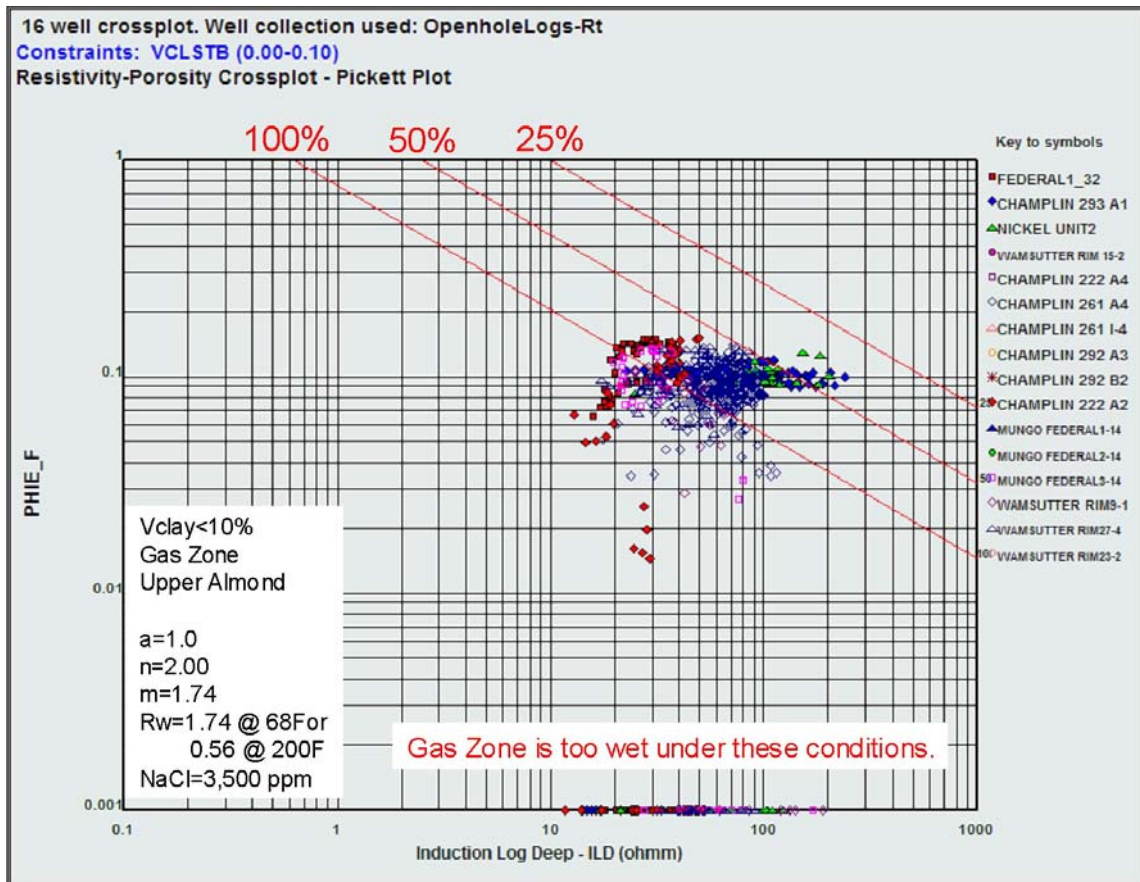
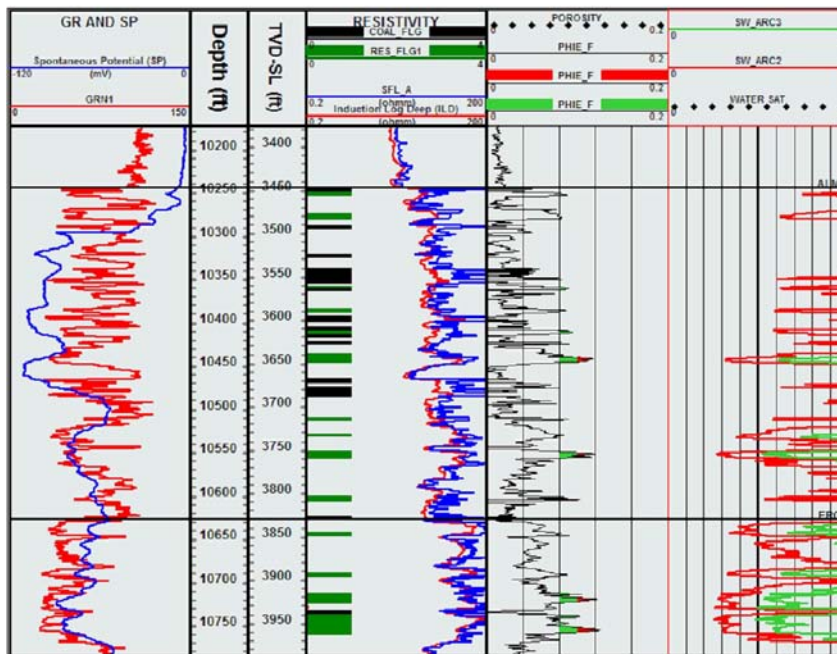


Fig. E-28. Pickett plot gas zone—  $R_w = 1.74$  @ 68°F



Champlin 293 A2

SW\_ARC2 (Low  
Rw model)

a=1.0  
n=2.00  
m=1.74  
Rw=0.68 @ 68F  
NaCl=13,000 ppm

SW\_ARC3 (High Rw  
model)

a=1.0  
n=2.00  
m=1.74  
Rw=1.74 @ 68F  
NaCl=13,000 ppm

If the low Rw model is used, the entire section calculates free gas including known water-producing zones in the Ericson. If the high Rw model is used, all sands calculate wet (>60% Sw).

**Fig. E-29. Water saturation models**

With these parameters, Pickett plots show the gas-bearing intervals to calculate 25%-60% water saturation (fig. E-30).

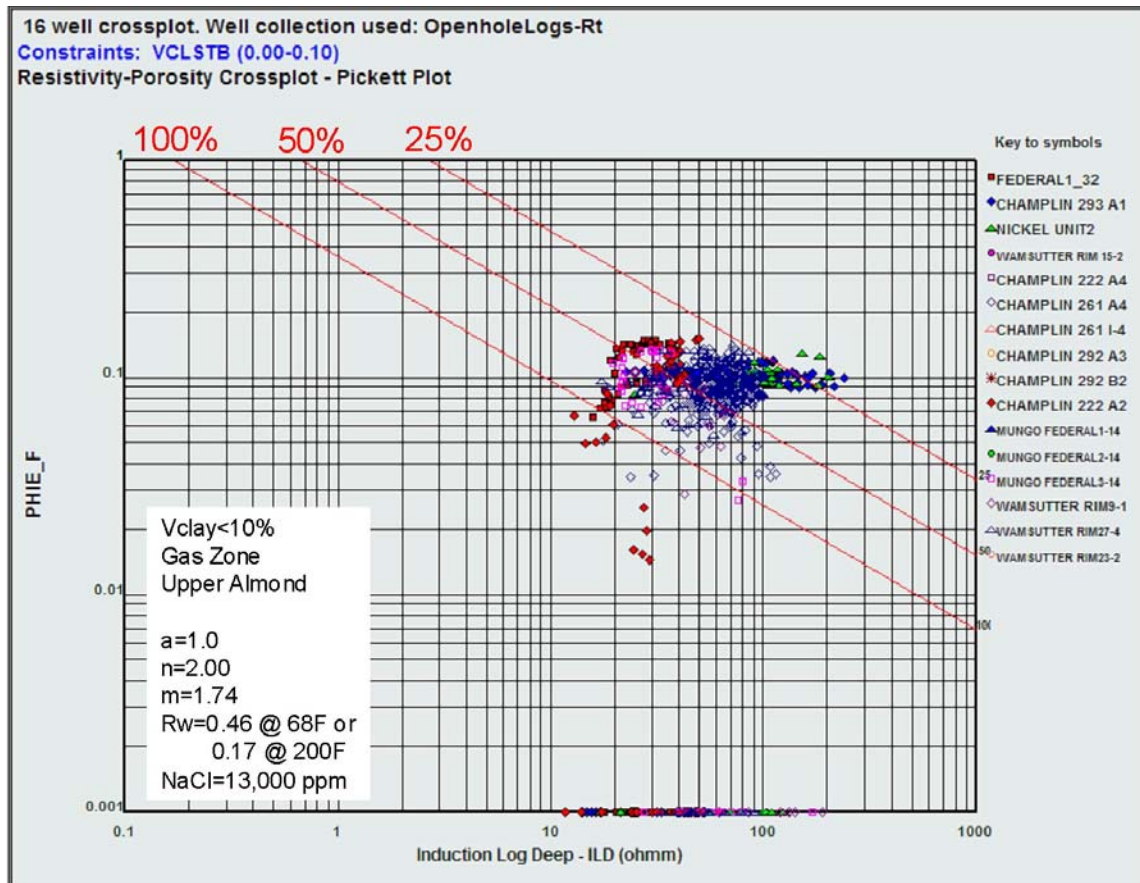


Fig. E-30. Pickett plot gas zone –  $R_w = 0.46$  @ 68F

Whereas the water salinity is known to change, the problem is how to identify where this change occurs. Two methods were developed to determine the fluid in the rock.

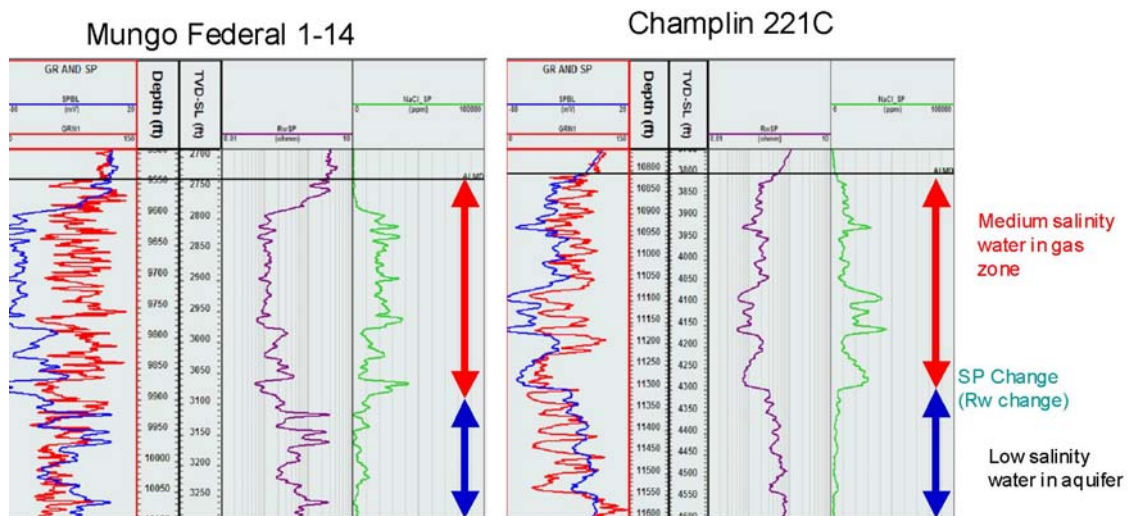
The first and more consistent method uses the SP curve. Most of the wells in the field use fresh water-based drilling mud. In permeable sands, where the formation water is more saline than the mud filtrate, the SP will read negative (1972 Schlumberger).

Where the formation water becomes less saline, the SP will read less negative or even positive. Therefore, the SP should be a good indicator of formation water salinity changes.

An apparent water resistivity analysis of the SP curve in wells Champlin 221C and Mungo Federal 1-14 clearly shows a change in water resistivity at the SP inflection (fig. E-31). Although the absolute  $R_w$  determination is not quite the same as the 3,500 ppm NaCl water samples, the change is clearly detected.

The SP- $R_w$  calculation is affected by the baseline shifting procedure and by the presence of bicarbonate, which is common in these rocks (720 to 2,600 ppm). Although the SP is generally reliable, it is strongly influenced by the resistivity of the mud filtrate, the operator and the operating conditions.

As a result, it sometimes does not have sufficient character to identify the  $R_w$  change.



It is difficult to exactly calibrate  $R_w$  from the SP curve due to

- Subjectivity in baseline shifting SP curve
- Variable amount of Bicarbonate in the water (700-2600 ppm)

Despite difficulties, SP to  $R_w$  calculations show a dramatic shift in water salinity in the upper and lower parts of the formation.

$R_w$  may be even more variable than water saturation model used in this study.

- Confirmed by variability in collected water analyses.

**Fig. E-31. SP- $R_w$**



In cases where the SP is not present or useful, the resistivity can sometimes be utilized. Since the sands are low permeability rock, capillary effects will draw the mud filtrate deep into the formation, which will affect the shallow resistivity measurement. In this case, the ratio between the shallow and deep resistivity should depict the water resistivity change.

The water in the gas zone is generally more saline than the aquifer water. Even though the zone is gas-bearing, water still takes up 25%-50% of the pore space. If the mud filtrate is sufficiently fresh, the shallow resistivity should read higher than the deep resistivity, and the  $R_{deep}/R_{shallow}$  separation will be large. Since both the mud filtrate and aquifer water are relatively fresh, the  $R_{deep}/R_{shallow}$  ratio will be lower.

This can be observed in well Cathedral Federal 3-2, Champlin 292 A1, Champlin 292 A2, Champlin 222 A1, and Wamsutter Rim 9-1 (figs. E-32 through E-36), where the change in resistivity ratio corresponds to the SP deflection.

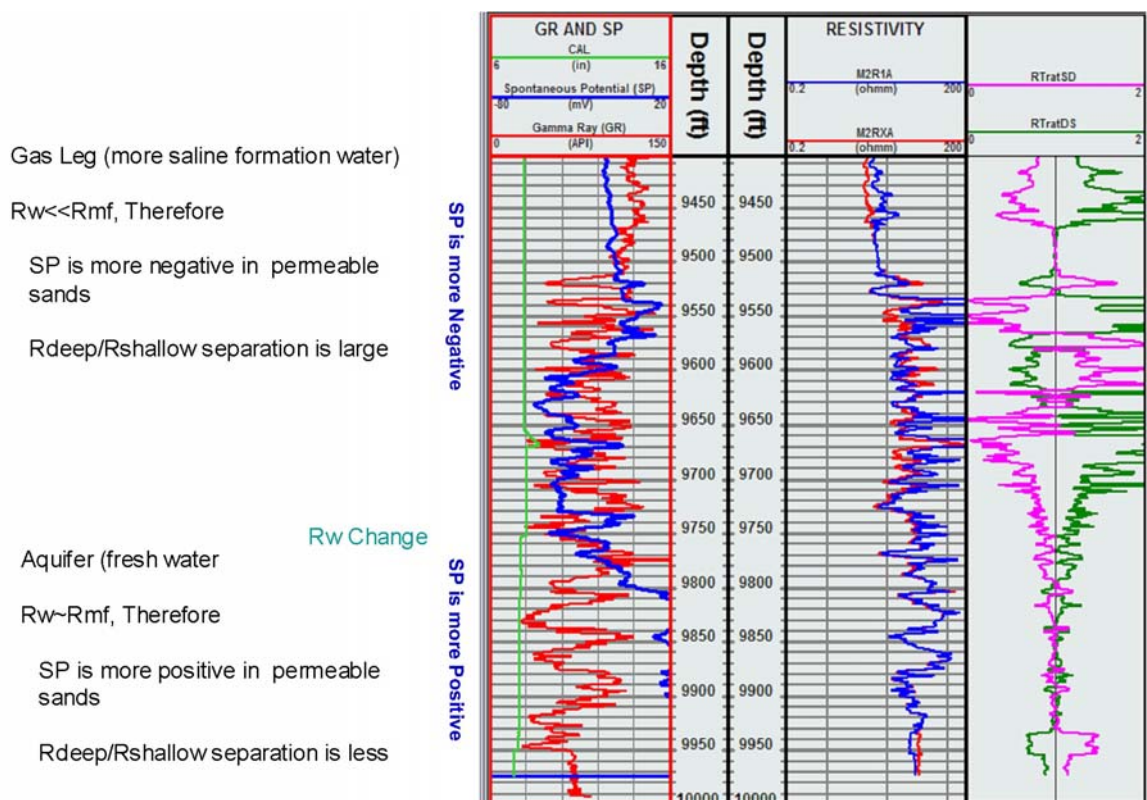


**Fig. E-32.  $R_w$  Change: Cathedral Fed 3-2**

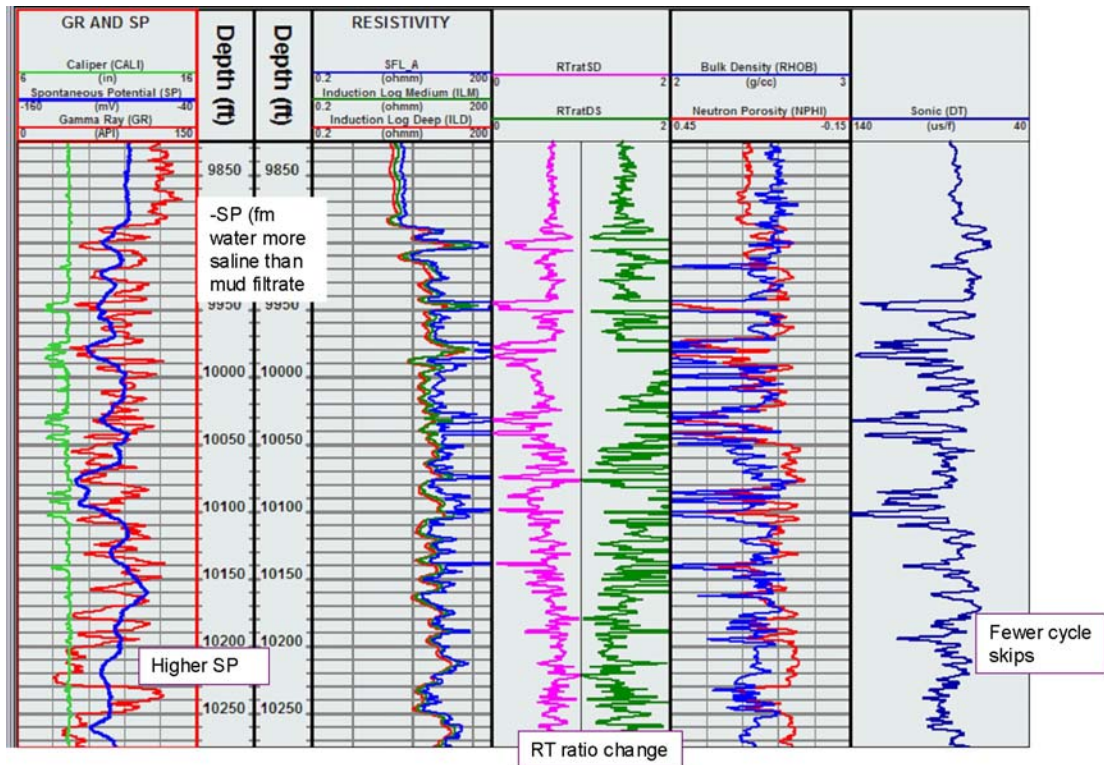


Fig. E-33. Rw Change: Champlin 292 A1

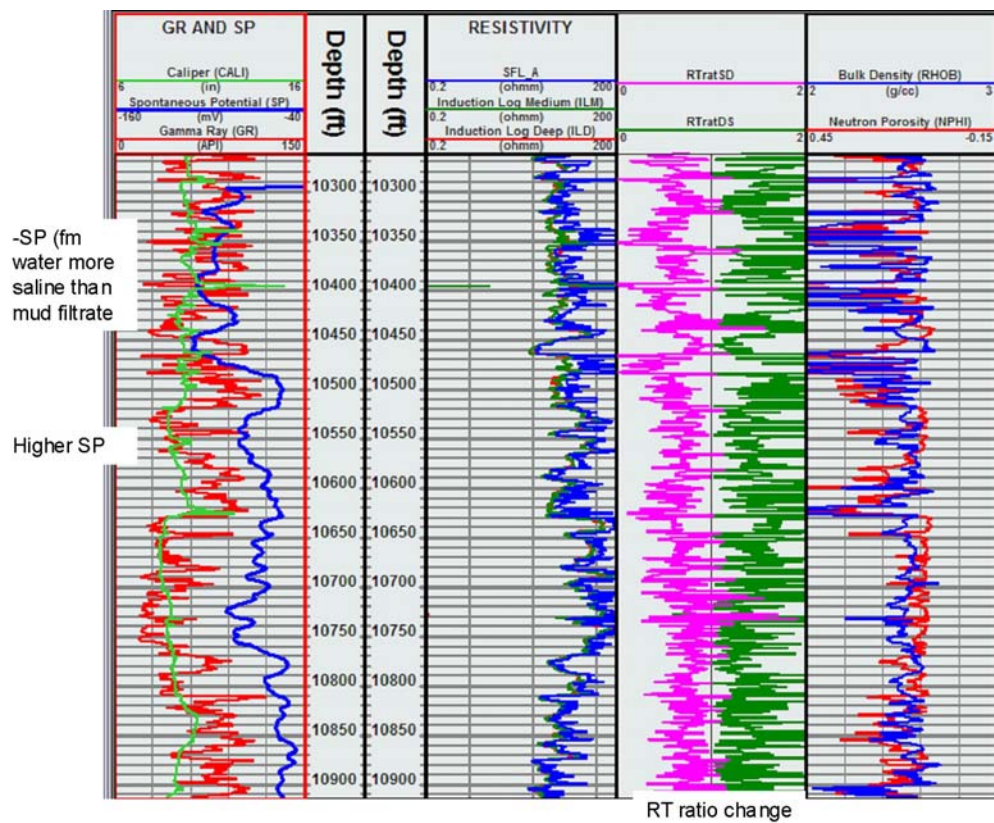


Fig. E-34. Rw Change: Champlin 292 A2



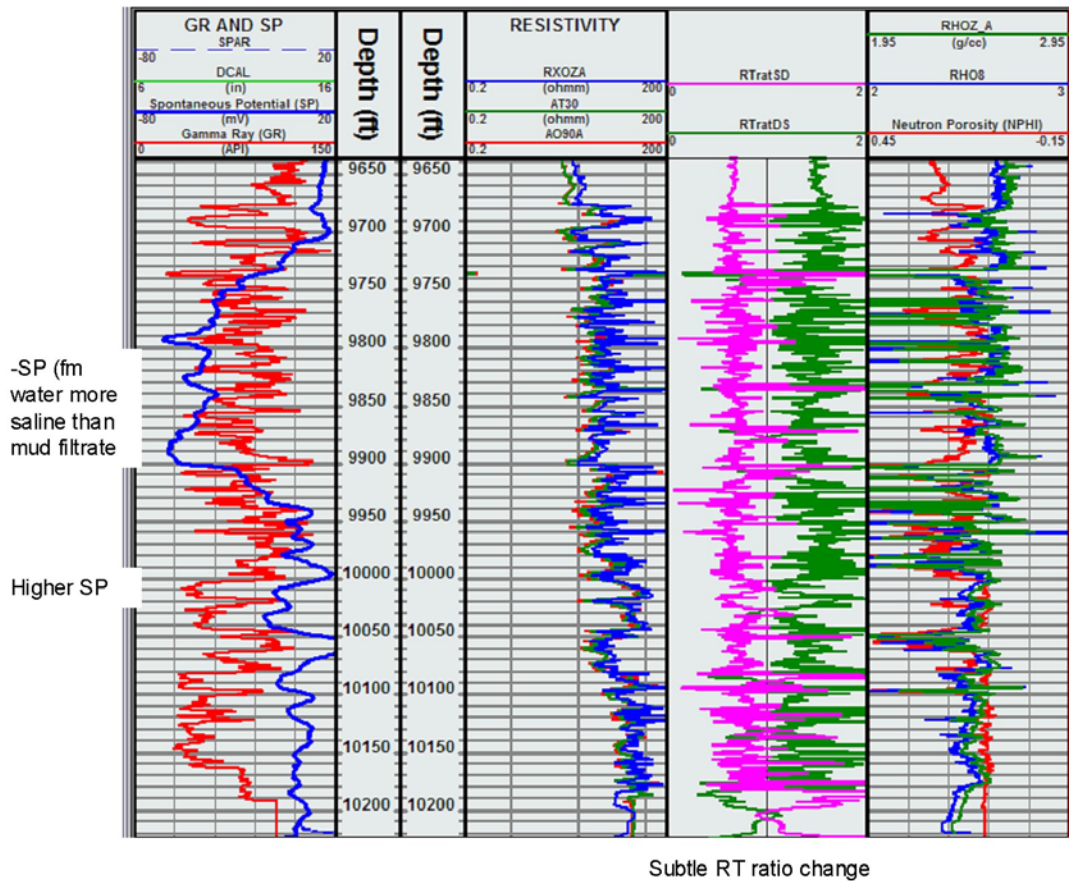


Fig. E-35. Rw Change: Wamsutter Rim 9-1

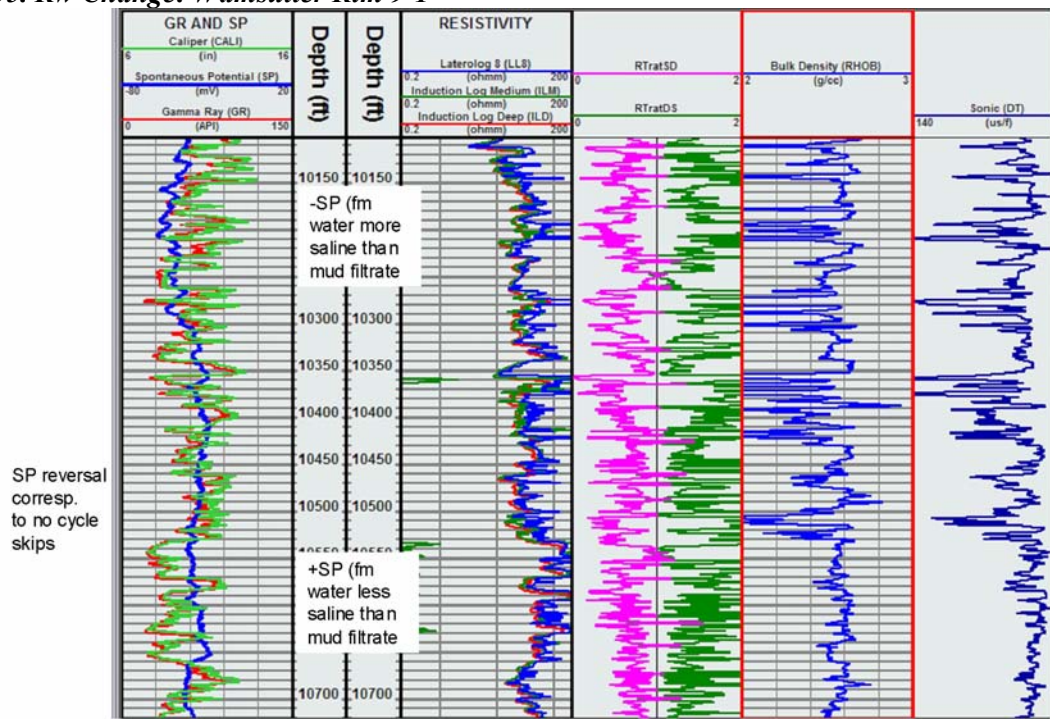


Fig. E-36. Rw Change: Champlin 222 A1





**Table E-14. Initial Production tests *above* the gas-water boundary**

< 10 BWPD	17 tests
11-20 BWPD	3 tests
21-30 BWPD	2 tests

**Table E-15. Initial Production tests *below* the gas-water boundary**

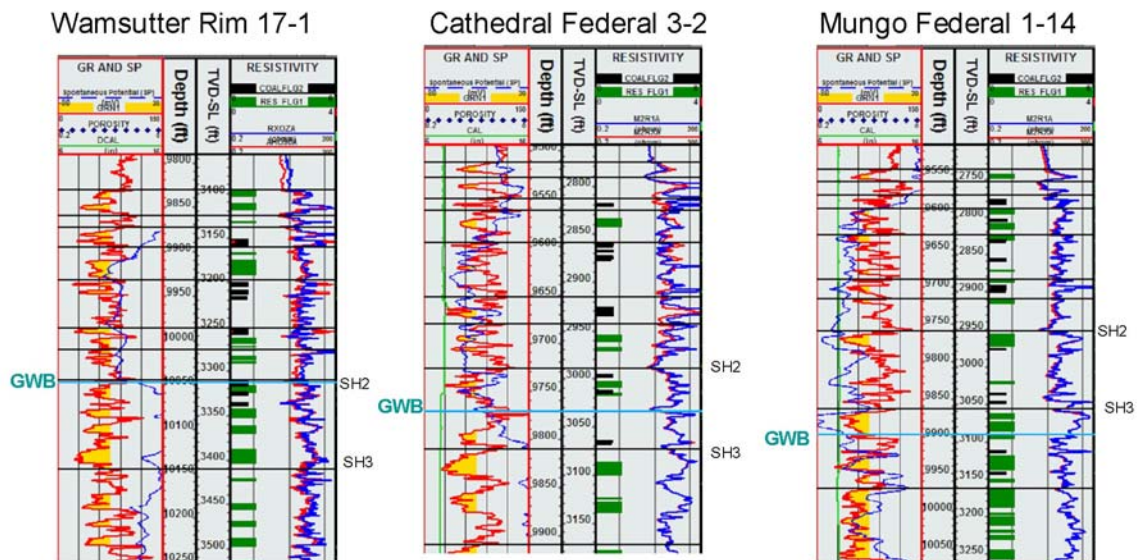
<25 BWPD	4 (tight rock or coal) & 3 (suspect)
25-50 BWPD	2 tests
>50 BWPD	20 tests

Since intervals were perforated over thick sections of sand, the deep tests produced both water and gas. In general, where the interval was perforated above the estimated gas-water boundary, tests produced less than 10 BWPD, and 30 BWPD at most. When perforated below the gas-water boundary, a majority of the tests produced 50-200 BWPD.

Seven tests produced less than 25 BWPD. Four of these were perforated in tight sands and shales below the contact, so little fluid would be produced unless a fracture set was intersected. The other three tests are suspect—since although they were perforated in good sands, the operator soon plugged back above the estimated gas-water boundary. In the other tests, nearby wells reported high water flows from the same sands, and it is presumed that water rates may be misreported.

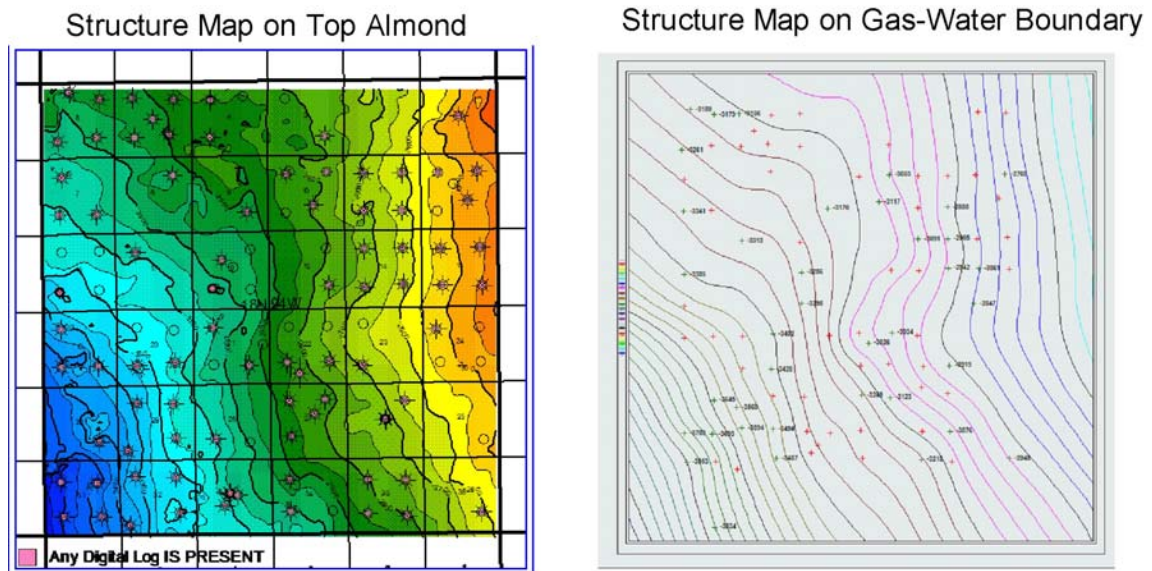
In wells lacking an SP and/or the resistivity ratio is not useful,  $R_w$  changes are estimated based on the location in surrounding wells. The gas-water interface is a boundary rather than an actual contact. In most parts of the field it is at or near the ALMD\_SH2 pick. As a result, when mapped, the gas-water interface is sloping, and suspected to be stratigraphically controlled (figs. E-38 and E-39). The ALMD\_SH2 is generally the first occurrence of significant coals in the section. Although some coals are found deeper in the ALMD\_SH3 section, they are intermittent, and usually thin.

The association of gas with the coals may indicate that the coals are the local source rock. At the same time, the limited lateral extent of the sands makes this reservoir a series of small traps requiring close well spacing to properly exploit. In more continuous sands like the Ericson, the reservoir quality is so good that any moving gas would continue to migrate updip to a higher point on the structure.



Gas-Water Boundary is picked based on SP and/or Resistivity curves.  
 Generally near Almd\_SH2 and Almd\_SH3 picks in this township.  
 Usually appears near first significant appearance of coals, which is a presumed local gas source.  
 Follows dipping structure, but not rigorously; therefore, is a boundary between discontinuous gas-charged & aquifer sands rather than an actual contact.

**Fig. E-38. Gas-water boundary**



Gas-Water Boundary follows dipping structure, but not rigorously; therefore, is a boundary between discontinuous gas-charged & aquifer sands rather than an actual contact.

**Fig. E-39. SP-GWC structure map**

## Water Saturation

According to the Siberia Ridge 5-2 core data (1998 Geoquest), the cementation factor ( $m$ ) should be 1.79. This measurement was refined to 1.74 from Pickett plots, and used for both the Archie and Simandoux water saturation equations. The cementation factor corrected for excess conductivity ( $m^*$ ) is 2.01 based on the Siberia Ridge core, and is used in the Waxman-Smiths equation.

The Siberia Ridge 5-2 core data shows the saturation exponent ( $n$ ) should be 1.52. This measurement is considered too low, and revised to 2.00 based on Pickett Plot modeling (figs. E-27 and E-30) for both the Archie and Simandoux water saturation equations. The cementation factor corrected for excess conductivity ( $n^*$ ) is 2.05 based on the Siberia Ridge core, and is used in the Waxman-Smiths equation.

The Dean Stark core data is too low to be realistic (<20%). This may be due to the possibility that it is actually a weight loss analysis rather than a real Dean Stark measurement. This technique normally reads low in tight rocks (2003 Jeff Craig)

Another possibility is that the sample is over-dried in a convection oven. These are clay-rich sands so the clay-bound water may have evaporated. This will cause the water saturations to read artificially low. Because the Dean Stark data is too low, the capillary pressure curves are used as guides. In this type of low permeability rock, the capillary pressure data suggests that the water saturation should range 32-67% (fig. E-40).

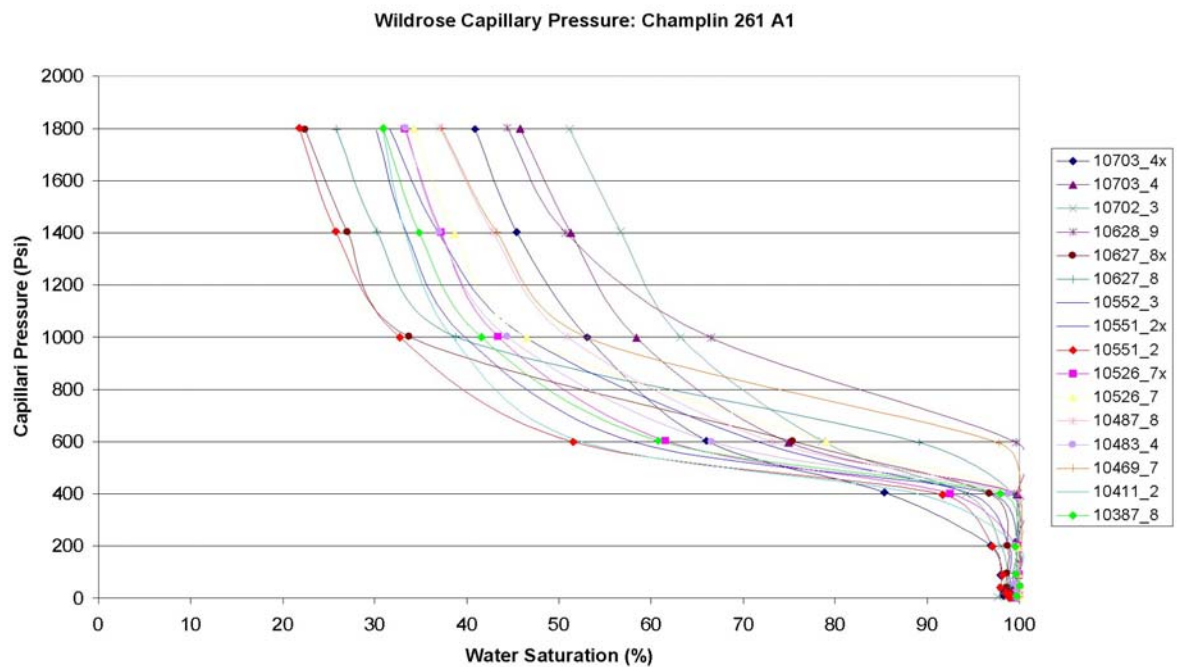


**Fig. E-40. Capillary pressure curves**



Since Dean Stark analysis and capillary pressure measurements are not conclusive, three methods were used to determine water saturation.

These include the Archie method, the Simandoux equation and Waxman-Smiths, which are displayed in fig. E-41.

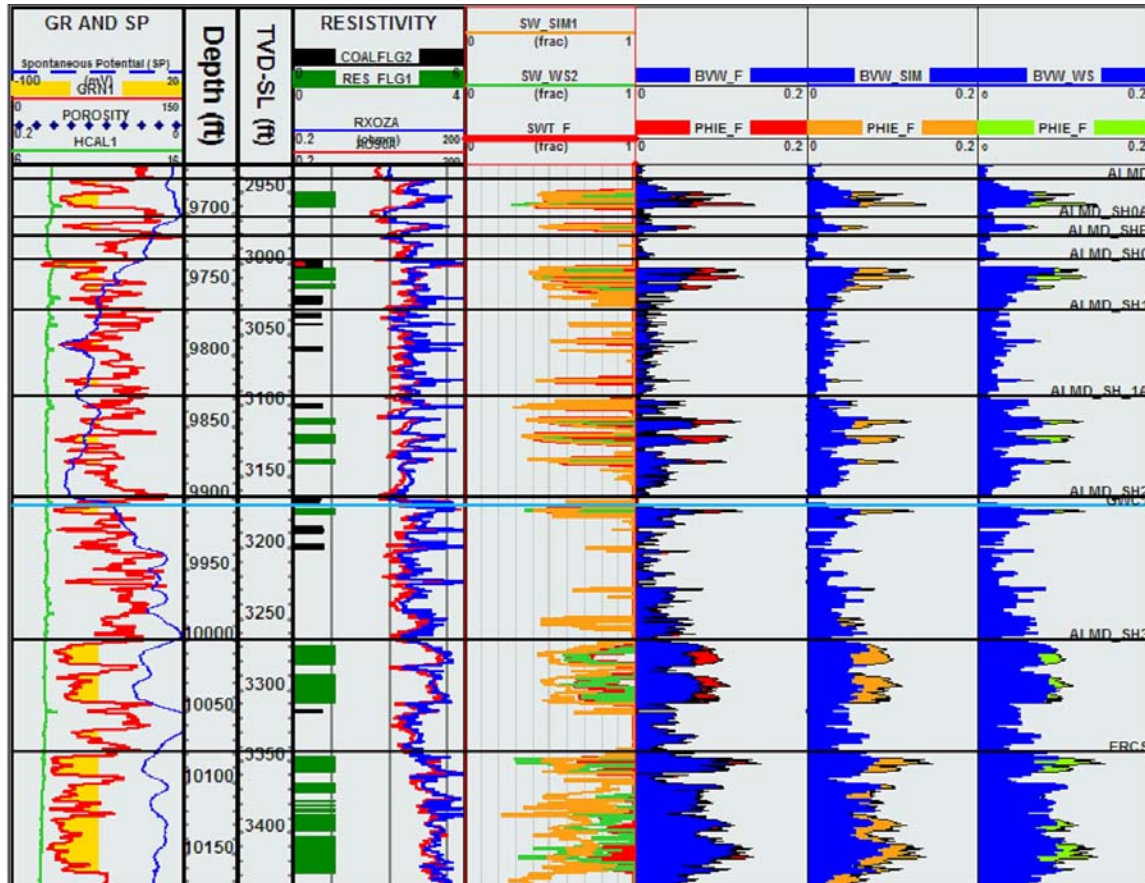


*Fig. E-41. Water Saturation Models: Wamsutter Rim 9-1*



Table E-16 is the Archie equation with the parameters used to determine water saturation.

**Table E-16. Archie equation parameters to determine water saturation**

$SW\_ARC = ((a \cdot R_w) / ((PHIE\_F^m) \cdot R_t))^{(1/n)}$   
 $a = 1.00$   
 $m = 1.74$  (Almond; from data fit, Siberia Ridge 5-2 core data)  
 $m = 2.00$  (Ericson; from data fit)  
 $n = 2.00$  (Almond & Ericson)  
 $R_w = 0.46$  @ 68° F (13000 ppm NaCl; above  $R_w$  change)  
 $R_w = 1.74$  @ 68° F (3500 ppm NaCl; below  $R_w$  change)  
 $R_t$  = True formation resistivity  
 $PHIE\_F$  = Final effective porosity

The Archie method results in values ranging 25%-60%  $S_w$  in gas-saturated reservoir quality sandstone, which is similar to that displayed in the capillary pressure range (32%-67%).

The Simandoux method as defined in the Terrasciences (2004) software uses the equation in Table E-17, with the same parameters as used in the Archie equation (Table E-16).

**Table E-17. Simandoux method to determine water saturation**

$SW \text{ (Simandoux)} = (((Ro \cdot (1 - V_{clay}) / R_t) + (X^2))^{0.5} - X)^{(2/n)}$   
Where:  $X = Ro \cdot V_{sh} \cdot (1 - V_{clay}) / (2 \cdot R_{sh})$   
 $Ro = (a \cdot R_w) / (PHIE^m)$   
 $V_{clay}$  = from VCLSTB curve  
 $R_{sh} = 10 \text{ ohm-m}$  (from logs)

The Simandoux equation takes into account the dispersed clay distribution. It is the most optimistic of all the methods that use an effective porosity. Fig. E-42 shows the relationship between SW (Archie) and SW (Simandoux).

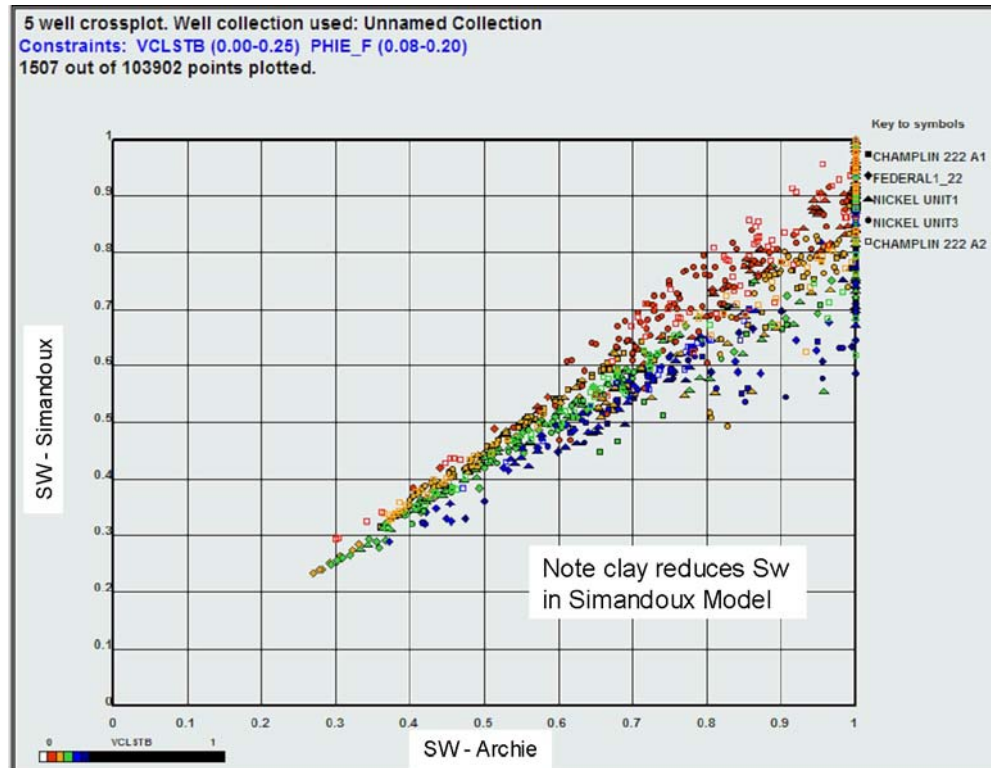


**Fig. E-42. Archie vs. Simandoux crossplot**

In general, the Simandoux equation has lower water saturations and shows more residual gas in the wet zones than the Archie equation.

The Waxman-Smits method (Table E-18) also accounts for dispersed clays, and uses the equation in the Terrasciences software (2004).

**Table E-18. Waxman-Smits method to determine water saturation**

$$SW \text{ (Waxman-Smits)} = S_{wn}^* = (F * R_w) / (R_t * (1 + R_w * B * Q_v / S_w))$$

Where:

B is the specific counterion activity. B is calculated by Waxman-Smit using  $B = (-1.28 + 0.225 * ZT - 0.0004059 * ZT * ZT) / (1 + (R_w * 1.23) * (0.045ZT - 0.27))$  where ZT is a temperature gradient correction

Qv is the cation exchange concentration. Although CEC measurements were made, Co/Cw were not, so Qv could not be properly calibrated. fig. E-43 shows a relationship between porosity and CEC.

$$CEC = 25.881 * PHIE$$

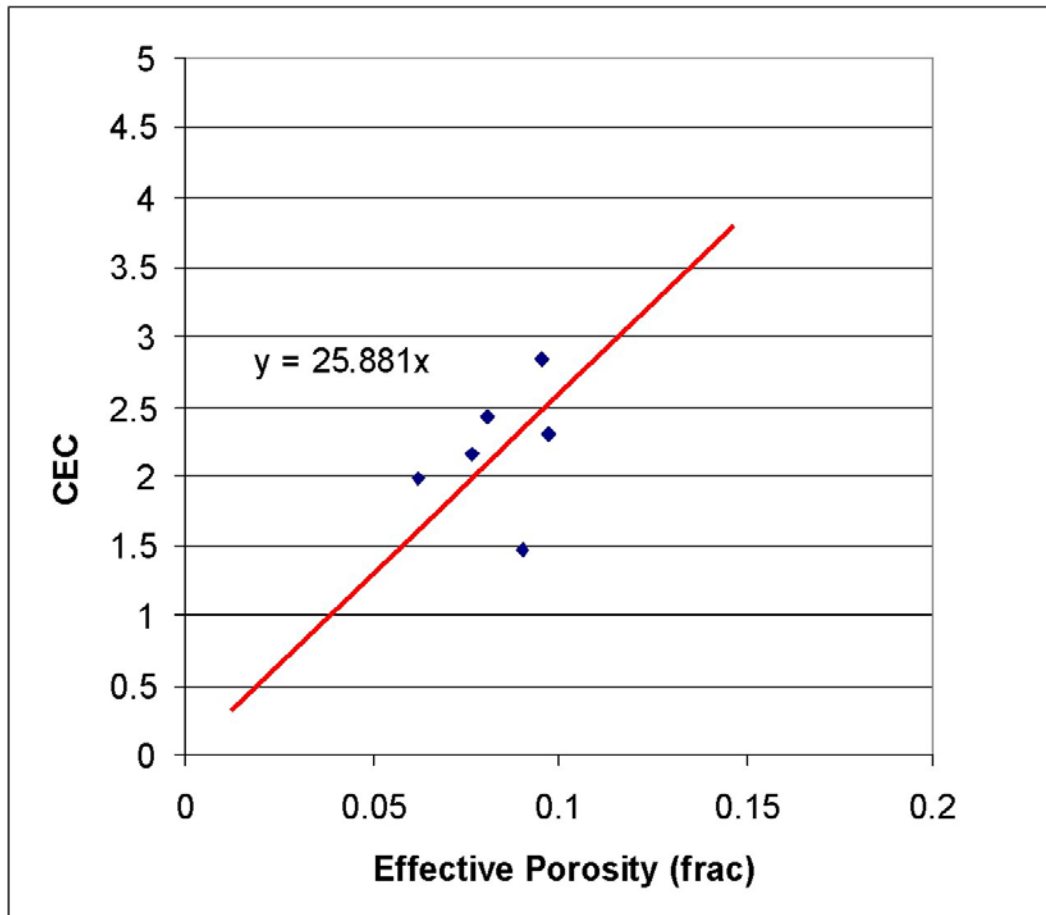


**Fig. E-43. Crossplot showing relationship between CEC-PHIE**

Based on this relationship and personal experience whereby illite-prone tight sands have a  $Q_v$  of approximately 0.25 in effective reservoir, the equation in Table E-19 is used.

**Table E-19. Equation: illite-prone tight sands have  $Q_v$  of approximately 0.25 in reservoir**

$$QV = CEC * PHIE$$

$$a = 1.00$$

$$m^* = 2.05 \text{ (from Siberia Ridge 5-2 core),}$$

$$n^* = 2.01 \text{ (from Siberia Ridge 5-2 core)}$$

$$R_w = 0.46 @ 68^\circ \text{ F (13000 ppm NaCl; gas zone)}$$

$$R_w = 1.74 @ 68^\circ \text{ F (3500 ppm NaCl; aquifer)}$$

$$R_t = \text{True formation resistivity}$$

$$PHIT = \text{Total porosity (not calibrated, so used effective porosity)}$$

$$F = a / (PHI^{m^*}) \text{ is the shaley sand formation factor}$$

Note that the Waxman-Smiths equation should use the total porosity, not effective porosity. But since a primary objective of this study was to build a reservoir model, the effective porosity was carefully calibrated and corrected for coal and washout; the total porosity was not.

$S_w$  is initially set to .5, the result of the equation is used as the new value of  $S_w$  and the calculation is repeated until  $(S_w - S_{wn}^*)$  is less than .0001

At low water saturations, the Waxman-Smits equation calculates higher gas saturation than the Archie equation (fig. E-44), but not as much gas as the Simandoux equation (fig. E-41).

At higher water saturations, the Waxman-Smits equation actually calculates lower gas saturation than the Archie equation, but this is most likely an artifact of how the  $Q_v$  is derived from the effective porosity. When total porosity is used higher gas saturations result.

It must be noted that the neither a total porosity nor a well-calibrated  $Q_v$  is used in this equation, so the Waxman-Smits method is most likely compromised.

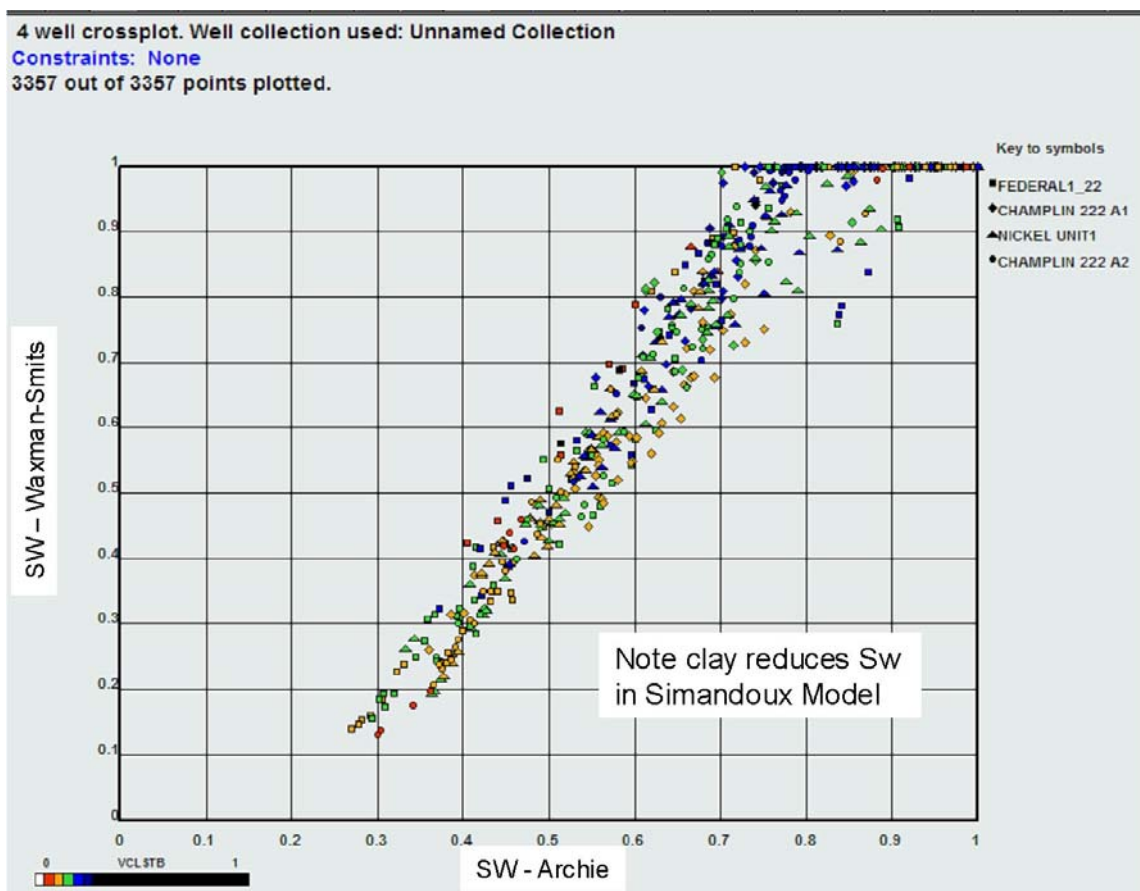


**Fig. E-44. Archie vs. Waxman-Smits crossplot**



## TDT Resistivity

Cased hole pulsed neutron water saturation is normally derived by calculating the neutron capture cross section sigma of the formation rock, formation water and hydrocarbon fluids. However, the Almond porosity is too low (<15%), the water is too fresh (<15,000 ppm NaCl), and the mineralogy is too complex to use the standard chartbook techniques.

Nevertheless, the TDT processed sigma curve has a strong correlation to the openhole deep resistivity (fig. E-45). In this study, the processed sigma curve is transformed into a deep resistivity curve by the equation in Table E-20. The results are shown in figs. E-18 through E-20. This curve is then substituted into the Archie equation in the previous section as the deep resistivity to derive water saturation.

**Table E-20. Equation: processed sigma curve is transformed into a deep resistivity curve**

$$\text{TDT\_Rt} = 279.95 * (e^{(-0.1376 * \text{SIGMA})})$$

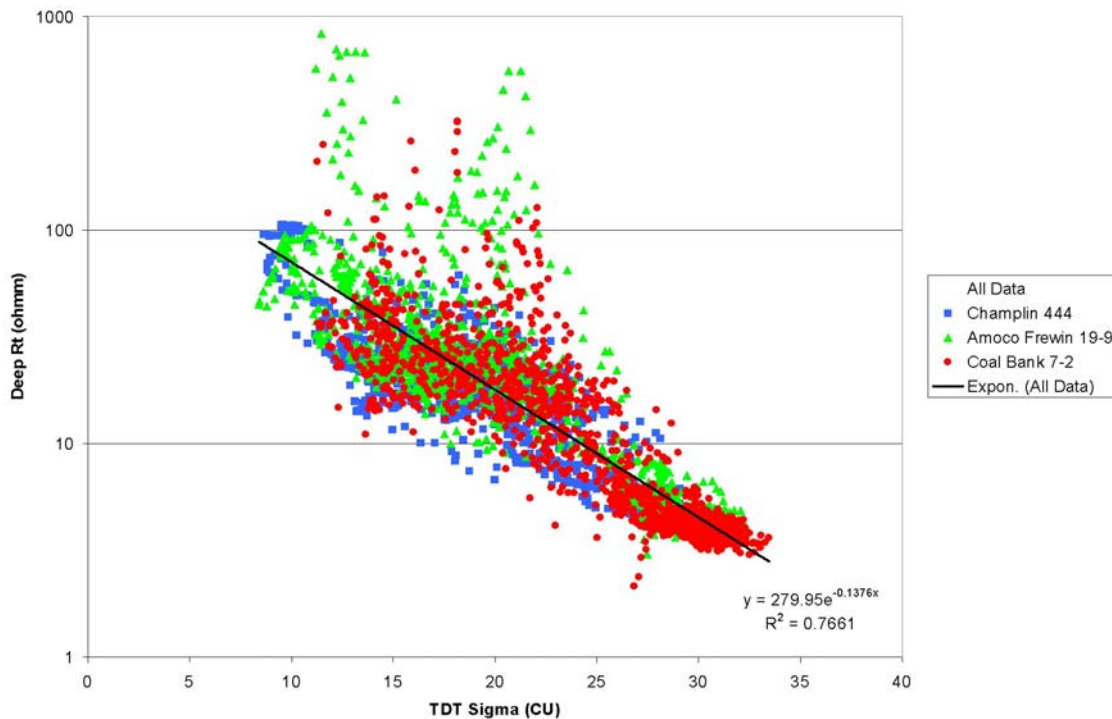


**Fig. E-45. TDT-Rt transform**

## Cutoffs

Based on the core data taken under pressure, no data points exceed 0.006md below 8% porosity (fig. E-21). Very few rocks will flow significant hydrocarbons below 0.01md. So the cutoffs in Table E-21 are used for this study. Additionally, with few exceptions, most of the capillary pressure curves cluster below 60% water saturation for any meaningful column heights.

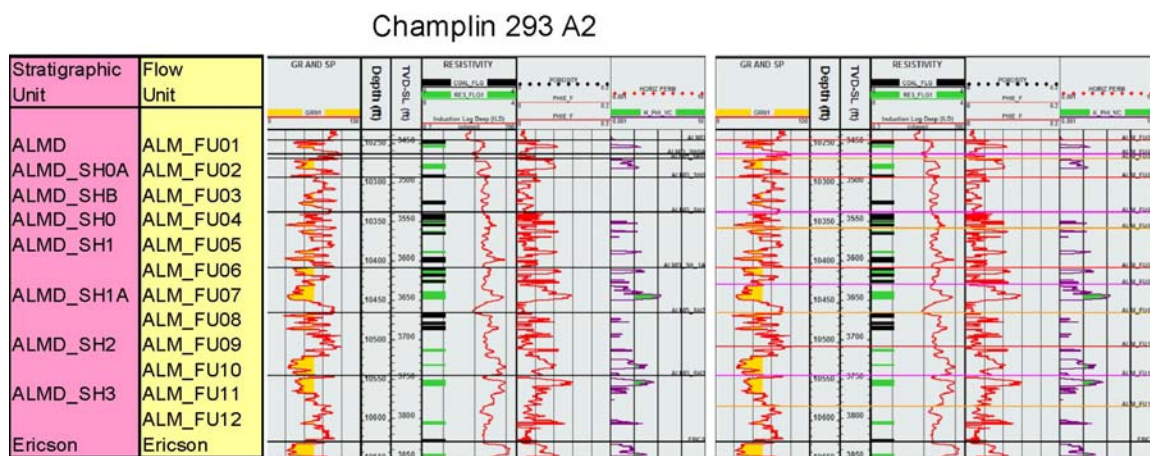
**Table E-21. Cutoffs**

Reservoir Cutoffs: Porosity > 8%
Vshale <50%
Pay Cutoff: Water saturation <60%

## Flow Units

Due to the layer cake nature and laterally discontinuous sands, flow units are based on the ARI stratigraphic nomenclature (fig. E-46). The most prominent picks for correlation is the ALMD\_SH1, ALMD\_SH2 and ALMD\_SH3, which are maximum flooding surface silts and shales, and appear to be laterally continuous over the study area.

Other subdivisions were made and are honored by the flow unit tops. Three other flow unit tops were also added to subdivide the large amount of section between ALMD\_SH1 and ALMD\_SH1A, ALMD\_SH1A and ALMD\_SH3, as well as ALMD\_SH3 and Erickson.



Flow Unit picks match ARI stratigraphic picks except where subdivided.

**Fig. E-46. Flow unit tops & stratigraphy**



## Conclusions

Despite mineralogical and textural complexity, we have a good petrophysical model for Vclay, Porosity, Permeability and Water Saturation:

- Works well in most openhole logs.
- Works well in approximately 60% of the cased hole logs.
- Requires extensive quality control.

Both porosity and Vclay affect permeability.

SP and resistivity ratios can be used to determine changes in formation water ( $R_w$ ):

- This may be related to the boundary between gas-charged sands and water-bearing sands.
  - Supported by initial production data.
- Useful for perforation/completion strategy and volumetrics.
- More work is needed to determine if this technique is valid outside this study area.

The change in  $R_w$  usually occurs near first appearance of significant coals in section.

Coals are believed to be a local source for gas.

Sands are a series of discontinuous lenses.